Eur. Phys. J. C (2024) 84:276
https://doi.org/10.1140/epjc/s10052-024-12613-z

THE EUROPEAN PHYSICAL JOURNAL C

Regular Article - Theoretical Physics

Revisiting the dynamics of interacting vector-like dark energy

Carlos Rodriguez-Benites[1,2,a], **Manuel Gonzalez-Espinoza**[3,4,b], **Giovanni Otalora**[5,c], **Manuel Alva-Morales**[2,6,d]

[1] Departamento Académico de Física, Facultad de Ciencias Físicas y Matemáticas, Universidad Nacional de Trujillo, Av. Juan Pablo II s/n, Trujillo, Peru
[2] GRACOCC and OASIS Research Groups, Facultad de Ciencias Físicas y Matemáticas, Universidad Nacional de Trujillo, Av. Juan Pablo II s/n, Trujillo, Peru
[3] Laboratorio de Cómputo de Física (LCF-UPLA), Departamento de Matemática, Física y Computación, Facultad de Ciencias Naturales y Exactas, Universidad de Playa Ancha, Subida Leopoldo Carvallo 270, Valparaiso, Chile
[4] Laboratorio de Didáctica de la Física, Departamento de Matemática, Física y Computación, Facultad de Ciencias Naturales y Exactas, Universidad de Playa Ancha, Subida Leopoldo Carvallo 270, Valparaiso, Chile
[5] Departamento de Física, Facultad de Ciencias, Universidad de Tarapacá, Casilla 7-D, Arica, Chile
[6] Escuela Profesional de Física, Facultad de Ciencias Físicas y Matemáticas, Universidad Nacional de Trujillo, Av. Juan Pablo II s/n, Trujillo, Peru

Received: 16 November 2023 / Accepted: 25 February 2024

Abstract We revise the dynamics of interacting vector-like dark energy, a theoretical framework proposed to explain the accelerated expansion of the universe. By investigating the interaction between vector-like dark energy and dark matter, we analyze its effects on the cosmic expansion history and the thermodynamics of the accelerating universe. Our results demonstrate that the presence of interaction significantly influences the evolution of vector-like dark energy, leading to distinct features in its equation of state and energy density. We compare our findings with observational data and highlight the importance of considering interactions in future cosmological studies.

1 Introduction

As revealed by observational data, the accelerated expansion of the universe is one of the most perplexing phenomena in modern cosmology. The prevailing explanation for this cosmic acceleration lies in an enigmatic entity known as dark energy, which constitutes a significant portion of the universe's energy content [1,2]. Exploring this entity offers immense potential to unravel the mysteries surrounding the fundamental building blocks and evolution of our vast Universe. The enigma of dark energy lies in its ability to drive the universe's accelerated expansion while eluding a comprehensive understanding of its physical origin and underlying mechanisms. This cosmic force permeates the fabric of space, counteracting the gravitational pull of matter and pushing galaxies farther apart. The precise nature of dark energy remains elusive, with candidates ranging from a cosmological constant, often associated with the energy of empty space [3,4], to dynamical scalar fields evolving over cosmic time [5] and modified gravity theories [6,7].

The simplest dark energy model, the ΛCDM model based on the cosmological constant and cold dark matter, faces theoretical issues like the fine-tuning problem tied to its energy scale, the cosmological constant problem, and the coincidence problem [8,9]. Furthermore, notable discrepancies have emerged between the ΛCDM model predictions using cosmic microwave background (CMB) data and independent local measurements [10–13]. Specifically, the Hubble constant H_0 from Planck data is 4.0σ to 6.3σ below local measurements [14], and the σ_8 clustering amplitude is higher than values from low-redshift observations [13,15–17]. Thus, these theoretical issues and recent observational findings have motivated the scientific community to explore and investigate alternative dark energy models. For instance, in the context of scalar field models and modified gravity theories, one can find in the literature non-minimally coupled scalar fields models [18–25], coupled dark energy [26–31], $f(R,\phi)$ [32–38], and $f(T,\phi)$ gravity [39–46], among others (see Refs. [2,7,47] and references therein).

Additionally, dark energy has not only been described using scalar fields but also through other types of fields, such as vector fields. In the context of generalized Proca theories, a massive vector field is introduced, which breaks the

[a] e-mail: cerodriguez@unitru.edu.pe (corresponding author)
[b] e-mail: manuel.gonzalez@upla.cl
[c] e-mail: giovanni.otalora@academicos.uta.cl
[d] e-mail: malvam@unitru.edu.pe

Published online: 17 March 2024

$U(1)$ symmetry. These vector theories belong to the class of time-like vector models. The homogeneous version of this vector field has a non-zero temporal component that is a function of cosmic time. For the most general case, its dynamics exhibit an asymptotic de Sitter attractor [48–53]. However, when the field is in its canonical form and minimally coupled to gravity, the equation motion becomes trivial, lacking dynamics and rendering it incapable of acting as a source of dark energy [54]. Furthermore, space-like vector has also been explored as a means to model inflation and dark energy [54–61]. While space-like models are generally associated with generating a highly anisotropic universe, there are specific scenarios where this challenge can be overcome. For instance, one of these scenarios involves the assumption of many randomly oriented vector fields, which, on average, results in an isotropic cosmological background, as described in Refs. [62,63]. Another method entails the consideration of three identical vector fields for each spatial direction, referred to as the 'cosmic triad,' a concept that also aligns with the background symmetry, as expounded upon [57].

Specifically, in Ref. [57], the author proposed a dark energy model based on three self-interacting vector fields minimally coupled to gravity, oriented in mutually orthogonal spatial directions, and sharing the same time-dependent length. This model, also known as the vector-like dark energy model, effectively drives the current accelerated expansion of the universe and introduces new tracking attractor solutions, making cosmic evolution insensitive to initial conditions [57] (see also Refs. [54,58,64,65]). Furthermore, in Ref. [66], the authors examined the dark-like energy model using the Noether approach, while in Ref. [67], they investigated the unified first law within this model.

As an interesting extension of this latter model, the Interacting Vector-like Dark Energy (IVDE) model has been proposed. For instance, in Ref. [68], the authors constructed a vector-like dark energy model for which an interaction between dark energy and a background perfect fluid was assumed. They identified two types of cosmological coincidence problems: the first asks why we live in an epoch where dark energy and dust matter energy densities are comparable; the second ponders why we exist in an epoch with $w_{de} < -1$. In this way, they found that these cosmological coincidence problems can be alleviated in such IVDE models. Also, in Ref. [69], the predictions of the IVDE model were compared with observational $H(z)$ data. In particular, they showed that the best IVDE models exhibit an oscillating feature for $H(z)$ and the equation-of-state parameter (EoS), crossing -1 around redshift $z \sim 1.5$.

The IVDE model offers a compelling avenue of exploration, providing a fresh approach to understanding the profound mysteries of dark energy. In this theoretical framework, dark energy is not an isolated entity but interacts with other cosmic components, such as dark matter, radiation, or neutrinos [70,71]. These interactions, mediated by a vector-like field, can potentially influence the cosmic expansion history and the formation and evolution of large-scale structures.

Understanding the properties and dynamics of IVDE is essential for several reasons. To the present work, IVDE may offer an alternative explanation for the accelerated expansion of the universe that extends beyond the standard cosmological model. By examining specific interaction mechanisms and studying their effects on cosmic evolution, we can gain deeper insights into the nature of dark energy and its role in shaping the cosmos [72,73]. Moreover, from a broader perspective in theoretical physics, IVDE has the potential to illuminate the complex interplay between dark energy and other fundamental forces and particles. For instance, exploring IVDE within the frameworks of quantum field theory and particle physics framework could reveal significant connections, thereby bridging the gaps between our understanding of the macroscopic universe and the microscopic realm of particles and fundamental interactions [74,75].

Therefore, the investigation of IVDE represents a captivating and vital avenue to understanding the nature and properties of dark energy. Through an in-depth analysis of IVDE, we can strive towards a comprehensive understanding of the nature and properties of dark energy while also advancing our knowledge of fundamental physics and the evolution of the cosmos. This research promises to unlock new horizons in our quest to comprehend the underlying mechanisms that govern the vastness of our universe.

In this paper, we study the cosmological dynamics of IVDE, analyzing its effects on the cosmic expansion history and the thermodynamics of the accelerating universe. In particular, we have performed a detailed phase space analysis, assuming several different functional forms for the coupling function Q between vector-like dark energy and dark matter. We extend previous studies in the literature [68] by including not only linear functional forms but also nonlinear functions for Q in terms of the energy densities. In the case of nonlinear functions, we demonstrate that the Q function can exhibit sign changes throughout the cosmic evolution.

The paper is organized as follows: In Sect. 2, we introduce the IVDE models, present the total action of the model, and derive the field equations in a general space-time. We then obtain the cosmological equations and define the effective dark energy, along with its coupling to dark matter. In Sect. 3 we reformulate the complete set of cosmological equations using new phase-space variables to derive a closed autonomous system. Furthermore, a detailed phase-space analysis of the model is performed, where we identify the corresponding critical points and their stability conditions. In Sect. 4, we corroborate our analytical findings by numerically solving the field equations. In Sect. 5, we explore the thermodynamic aspects of the interacting scenario within the context of IVDE models, determining the evolution of the

temperature of dark matter and dark energy as influenced by the coupling function Q. Finally, in Sect. 6, we summarize the results obtained.

2 Vector-like dark energy

The concept of "vector-like dark energy" refers to a "cosmic triad," as described in reference [57]. This triad consists of three identical vectors oriented in mutually orthogonal directions, ensuring the preservation of isotropy. In line with the approach presented in reference [57], we examine the scenario where vector-like dark energy is minimally coupled to gravity. The corresponding action can be expressed as follows:

$$S=\int \mathrm{d}^4x\sqrt{-g}\left[\frac{R}{2\kappa^2}-\sum_{a=1}^{3}\left(\frac{1}{4}F^a{}_{\mu\nu}F^{a\mu\nu}+V(A^{a2})\right)\right] +S_m+S_r, \tag{1}$$

where $\kappa^2=8\pi G$, with G being the gravitational constant, $F^a{}_{\mu\nu}=\partial_\mu A^a_\nu-\partial_\nu A^a_\mu$ and $A^{a2}=g^{\mu\nu}A^a_\mu A^a_\nu$. S_m is the action of matter S_r is the action of radiation. It is worth noting that the superscript a indicates each vector field constituting the cosmic triad.

Then, varying the action (1) with respect to the metric, we obtain the following equations:

$$\frac{G_{\mu\nu}}{\kappa^2}-\sum_{a=1}^{3}\left\{F^a{}_{\mu\rho}F^{a\rho}_{\ \ \nu}+2\frac{\mathrm{d}V}{\mathrm{d}A^{a2}}A^a_\mu A^a_\nu -g_{\mu\nu}\left[\frac{1}{4}F^a{}_{\mu\nu}F^{a\mu\nu}+V(A^{a2})\right]\right\}=2T^{(m)}_{\mu\nu}+2T^{(r)}_{\mu\nu}. \tag{2}$$

And, varying with respect to the cosmic triad A^a_μ we find the equation of motion

$$\partial_\mu(\sqrt{-g}F^{a\mu\nu})=2\sqrt{-g}\frac{\mathrm{d}V}{\mathrm{d}A^{a2}}A^{a\nu}. \tag{3}$$

Below, we detail the basic equations for the cosmic triad in a cosmological background.

2.1 Cosmological dynamics

We consider a spatially flat Friedmann–Lemaître–Robertson–Walker (FLRW) universe with metric:

$$\mathrm{d}s^2=-\mathrm{d}t^2+a^2(t)\delta_{ij}\mathrm{d}x^i\mathrm{d}x^j, \tag{4}$$

where a is the scale factor, a function of the cosmic time t. We also assume the following ansatz:

$$A^a_\mu=\delta^a_\mu A(t)a(t). \tag{5}$$

Thus, the modified Friedmann equations are given by

$$\frac{3H^2}{\kappa^2}=\frac{3}{2}(\dot{A}+HA)^2+3V+\rho_m+\rho_r, \tag{6}$$

$$-\frac{2\dot{H}}{\kappa^2}=2(\dot{A}+HA)^2+2A^2V_{,A^2}+\rho_m+\frac{4}{3}\rho_r, \tag{7}$$

and the motion equation of the vector field A:

$$\ddot{A}+3H\dot{A}+A\dot{H}+2AH^2+2AV_{,A^2}=0. \tag{8}$$

In the above, $V\left(A^2\right)$ represents the scalar potential, $H\equiv\dot{a}/a$ stands for the Hubble rate, where a dot denotes the derivative with respect to time, and a comma indicates derivative with respect to A^2. Furthermore, the functions ρ_i and p_i, with $i=m,r$ denoting either non-relativistic matter (comprising cold dark matter and baryons) or radiation, respectively, serve as the energy and pressure densities. It is important to note that in the equations mentioned earlier, we have already incorporated the respective barotropic equations of state, namely, $w_m=p_m/\rho_m=0$ and $w_r=p_r/\rho_r=1/3$.

Following Ref. [2] one can rewrite the Friedmann equations (6) and (7) in their standard form as

$$\frac{3H^2}{\kappa^2}=\rho_{de}+\rho_m+\rho_r, \tag{9}$$

$$-\frac{2\dot{H}}{\kappa^2}=p_{de}+\rho_{de}+\rho_m+\frac{4}{3}\rho_r. \tag{10}$$

Therefore, we can define the effective energy and pressure densities of the model as:

$$\rho_{de}=\frac{3}{2}(\dot{A}+HA)^2+3V, \tag{11}$$

$$p_{de}=\frac{1}{2}(\dot{A}+HA)^2-3V+2A^2V_{,A^2}. \tag{12}$$

On the other hand, from the conservation of the total energy-momentum tensor we have

$$\dot{\rho}+3H(\rho+p)=0, \tag{13}$$

each component (matter, radiation, and dark energy) satisfy (13) separately in a scenario without interaction. And, it is worth noticing that matter and radiation have standard behavior $\rho_m\sim a^{-3}$ and $\rho_r\sim a^{-4}$, respectively.

Additionally, we can define the effective dark energy EoS as

$$w_{de}=\frac{p_{de}}{\rho_{de}}. \tag{14}$$

It is also convenient to introduce the total equation-of-state parameter as

$$w_{tot}=\frac{p_{de}+p_r}{\rho_{de}+\rho_m+\rho_r}, \tag{15}$$

which is related to the deceleration parameter q through

$$q=\frac{1}{2}(1+3w_{tot}), \tag{16}$$

and, hence, it is easy to see that the acceleration of the Universe occurs for $q < 0$ or, equivalently, when $w_{tot} < -1/3$.

Finally, another set of cosmological parameters that can be introduced is the standard density parameters, which are defined as

$$\Omega_r \equiv \frac{\kappa^2\rho_r}{3H^2},\ \Omega_m \equiv \frac{\kappa^2\rho_m}{3H^2},\ \Omega_{de} \equiv \frac{\kappa^2\rho_{de}}{3H^2}, \tag{17}$$

and satisfy the constraint equation

$$\Omega_r + \Omega_m + \Omega_{de} = 1. \tag{18}$$

In what follows, we extend the previous analysis to include the interaction between vector-like dark energy and dark matter [76].

2.2 Interacting dark energy

We assume that the vector-like dark energy interacts with the dark matter through a phenomenological interaction term Q, according to [76]

$$\dot{\rho}_{de} + 3H(\rho_{de} + p_{de}) = -Q, \tag{19}$$
$$\dot{\rho}_m + 3H\rho_m = Q, \tag{20}$$
$$\dot{\rho}_r + 4H\rho_r = 0, \tag{21}$$

which preserves the total energy conservation law. By assuming this interaction between the dark components, the equation of motion (8) should be changed when $Q \neq 0$ and a new term due to Q will appear in its r.h.s. [68].

In the following section, we conduct a thorough phase-space analysis for this dark energy model. Specifically, we derive the corresponding autonomous system based on the set of cosmological equations (9), (10), (19), (20) and (21).

3 Phase-space analysis

We introduce the following set of dimensionless variables [2]:

$$x = \frac{\kappa\dot{A}}{\sqrt{6}H},\ y = \frac{\kappa\sqrt{V}}{\sqrt{3}H},\ \lambda = -\frac{V_{,A^2}}{\kappa^2 V},$$
$$u = \frac{\kappa A}{\sqrt{6}},\ \varrho = \frac{\kappa\sqrt{\rho_r}}{\sqrt{3}H},\ \Gamma = \frac{V_{,A^2A^2}V}{(V_{,A^2})^2}, \tag{22}$$

and the constraint equation:

$$3x^2 + 3y^2 + 3u^2 + 6ux + \varrho^2 + \Omega_m = 1. \tag{23}$$

Therefore, we obtain the dynamical system

$$\begin{aligned}
\frac{dx}{dN} &= \frac{1}{2}\Big[u^3(3-36\lambda y^2) + 9u^2x(1-4\lambda y^2) \\
&\quad + u(9x^2 + 3(4\lambda-3)y^2 + \varrho^2 - 1) \\
&\quad + x(3x^2 - 9y^2 + \varrho^2 - 3)\Big] - \frac{Q\kappa^2}{18(u+x)H^3}, \\
\frac{dy}{dN} &= \frac{1}{2}y\Big[u^2(3-36\lambda y^2) + 6(1-2\lambda)ux \\
&\quad + 3x^2 - 9y^2 + \varrho^2 + 3\Big], \\
\frac{d\varrho}{dN} &= \frac{1}{2}\varrho\Big[u^2(3-36\lambda y^2) + 6ux + 3x^2 - 9y^2 + \varrho^2 - 1\Big], \\
\frac{d\lambda}{dN} &= -12(\Gamma-1)\lambda^2 ux, \\
\frac{du}{dN} &= x,
\end{aligned} \tag{24}$$

where $N \equiv \ln a$ is the number of e-folds, and it is used as the temporal parameter since it is a function of the cosmic scale factor. Using the above set of phase space variables, we can also write:

$$\Omega_{de} = 3u^2 + 6ux + 3x^2 + 3y^2, \tag{25}$$
$$\Omega_m = 1 - 3u^2 - 6ux - 3x^2 - 3y^2 - \varrho^2, \tag{26}$$
$$\Omega_r = \varrho^2. \tag{27}$$

The equation of state (EoS) of dark energy $w_{de} = p_{de}/\rho_{de}$ can be rewritten as

$$w_{de} = \frac{u^2(1-12\lambda y^2) + 2ux + x^2 - 3y^2}{3(u^2 + 2ux + x^2 + y^2)}, \tag{28}$$

whereas the total EoS becomes

$$w_{tot} = u^2(1-12\lambda y^2) + 2ux + x^2 - 3y^2 + \frac{\varrho^2}{3}. \tag{29}$$

To obtain an autonomous system from the dynamical system (24), we need to define the potentials for the vector field. From now we concentrate on the exponential potential $V(A^2) \sim e^{-\kappa^2\lambda A^2}$. Below, we study the critical points and their stability properties for various interaction cases.

In the literature, various models have been explored where the function Q, which represents the interaction term, is considered as a function of energy densities and the Hubble parameter [76,77]. In this paper, we use three interacting scenarios: linear, non-linear, and a sign-changeable [78].

3.1 Critical points

In this section, we obtain the critical points from the conditions $dx/dN = dy/dN = d\varrho/dN = du/dN = 0$ [2]. Where, if we consider the definition of each dynamical variable (22), the critical points that are physically possible are given by $y_c \geq 0,\ \varrho_c \geq 0$ and $u_c \geq 0$.

Consequently, we find the critical points for each interaction term:

3.1.1 Case I: $Q = 3\alpha H\rho_m$

Using the above set of phase space variables, we can rewrite the interaction term as:

$$Q = \frac{9\alpha H^3(1 - 3u^2 - 6ux - 3x^2 - 3y^2 - \varrho^2)}{\kappa^2}. \tag{30}$$

Critical points of the system (24) with interaction case (30) are shown in Table 1 and the values of their cosmological parameters in Table 2. Also, in this subsection and so on, we define $\Omega_{de}^{(r)}$ and $\Omega_{de}^{(m)}$ as the amount of dark energy during a radiation and dark matter domination era, respectively.

The critical point a_R corresponds to a scaling radiation era, where $\Omega_{de}^{(r)} = u_c^2$. When $u_c = 0$, we obtain the radiation-dominated solution with $\Omega_r = 1$ and $w_{de} = w_{tot} = 1/3$. For $u_c \neq 0$, this point represents a scaling radiation era. Thus, to satisfy the early constraint imposed by the physics of big bang nucleosynthesis (BBN) and ensure $\Omega_{de}^{(r)} < 0.045$ [79,80], we need to have $u_c < 0.122$.

The critical point c represents a dark energy-dominated solution with a de Sitter EoS, where $w_{de} = w_{tot} = -1$. As a result, this critical point yields accelerated expansion for all parameter values.

On the other hand, for $\alpha = 0$, the critical point labeled as b_M represents a matter-dominated era, with $\Omega_m = 1$ and $w_{de} = w_{tot} = 0$. In this case, the energy density of matter dominates the universe, and the EoS parameter for dark energy ($w_{de} = 1/3$) and the total EoS parameter (w_{tot}) is zero. For $\alpha \neq 0$, we have a scaling matter era which is constrained to satisfy $\Omega_{de}^{(m)} < 0.02$ (95% CL), at redshift de $z \approx 50$, according to CMB measurements [81]. Thus, this leads us to the constraint $0 < \alpha < 0.01$, which is also compatible with $0 < \Omega_m < 1$.

3.1.2 Case II: $Q = 3\beta H\frac{{\rho_m}^2}{\rho_m + \rho_{de}}$

With the phase space variables mentioned earlier, we express the interaction term in the following form

$$Q = \frac{9\beta H^3\left[3(u + x)^2 + 3y^2 + \varrho^2 - 1\right]^2}{\kappa^2\left(1 - \varrho^2\right)}. \tag{31}$$

The critical points of the system described in Eq. (24) under the interaction case given by Eq. (31) are presented in Table 3, along with the corresponding values of their cosmological parameters in Table 4.

The critical point labeled as d_R corresponds to a scaling radiation era, characterized by $\Omega_{de}^{(r)} = u_c^2$. When $u_c = 0$, we obtain the radiation-dominated solution with $\Omega_r = 1$ and $w_{de} = w_{tot} = 1/3$. For $u_c \neq 0$, this point describes a scaling radiation era. To satisfy the early constraint imposed by the physics of big bang nucleosynthesis (BBN) and ensure $\Omega_{de}^{(r)} < 0.045$ [79,80], the condition $u_c < 0.122$ must be met.

On another note, for $\beta = 0$, the critical point denoted as e_M represents a matter-dominated era, where $\Omega_m = 1$ and $w_{de} = w_{tot} = 0$. In this scenario, the energy density of matter dominates the universe, resulting in a dark energy EoS parameter of $w_{de} = 1/3$ and a total EoS parameter of $w_{tot} = 0$. For $\beta \neq 0$, we have a scaling matter era. Applying the constraint $\Omega_{de}^{(m)} < 0.02$ (95% CL), at redshift de $z \approx 50$, according to CMB measurements [81], we obtain $0 < \beta < 0.01$, which is also compatible with $0 < \Omega_m < 1$.

Moreover, the critical point labeled as f signifies a dark energy-dominated solution characterized by a de Sitter EoS, with $w_{de} = w_{tot} = -1$. Consequently, this critical point leads to accelerated expansion regardless of the parameter values.

Finally, the points f_1 and f_2 are not physically viable, because the fractional density is constrained by $0 < \Omega_m < 1$, meaning that, $0 < -1/\beta < 1$ or $\beta < -1$, but β must be positive and small to obtain a matter-dominated era as described by point e_M. Therefore, aiming to reproduce the standard thermal history of the universe, points f_1 and f_2 are identified as unphysical.

3.1.3 Case III: $Q = \frac{3}{2\kappa^2}\eta H^3(1 + \Omega_r - 3\Omega_{de})\Omega_m$

Given the above set of phase space variables, we express the interaction term as follows:

$$Q = \frac{3\eta H^3\left(9(u + x)^2 + 9y^2 - \varrho^2 - 1\right)\left(3(u+x)^2 + 3y^2 + \varrho^2 - 1\right)}{2\kappa^2}. \tag{32}$$

Critical points of the system (24) with interaction case (32) are shown in Table 5 and the values of their cosmological parameters in Table 6

The critical point denoted as g_R corresponds to a scaling radiation era, where $\Omega_{de}^{(r)} = u_c^2$. When $u_c = 0$, it gives rise to the radiation-dominated solution with $\Omega_r = 1$ and $w_{de} = w_{tot} = 1/3$. The case $u_c \neq 0$, corresponds to a scaling radiation era. Therefore, to meet the early constraint imposed by the physics of big bang nucleosynthesis (BBN) and ensure $\Omega_{de}^{(r)} < 0.045$ [79,80], the condition $u_c < 0.122$ must be satisfied.

Conversely, when $\eta = 0$, the critical point labeled as h_M represents a matter-dominated era, characterized by $\Omega_m = 1$ and $w_{de} = w_{tot} = 0$. In this scenario, the energy density of matter dominates the universe, leading to a dark energy EoS parameter of $w_{de} = 1/3$. In contrast, the total equation of the state parameter remains at $w_{tot} = 0$. When $\eta \neq 0$, this point represents a scaling matter era. Thus, from constraint

Table 1 Critical points for the autonomous system

Name	x_c	y_c	ϱ_c	u_c
a_R	0	0	$\sqrt{1-3{u_c}^2}$	u_c
b_M	0	0	0	$\sqrt{\alpha}$
c	0	$\frac{1}{\sqrt{3\lambda}}$	0	$\sqrt{\frac{\lambda-1}{3\lambda}}$

Table 2 Cosmological parameters for the critical points in Table 1

Name	Ω_{de}	Ω_m	Ω_r	w_{de}	w_{tot}
a_R	$3{u_c}^2$	0	$1-3{u_c}^2$	$\frac{1}{3}$	$\frac{1}{3}$
b_M	3α	$1-3\alpha$	0	$\frac{1}{3}$	α
c	1	0	0	-1	-1

Table 3 Critical points for the autonomous system. Where $F_\beta = \beta^2(\lambda-1)^2+\beta\lambda(2\lambda+1)+\lambda^2$

Name	x_c	y_c	ϱ_c	u_c
d_R	0	0	$\sqrt{1-3{u_c}^2}$	u_c
e_M	0	0	0	$\sqrt{\frac{\beta}{1+3\beta}}$
f	0	$\frac{1}{\sqrt{3\lambda}}$	0	$\sqrt{\frac{\lambda-1}{3\lambda}}$
f_1	0	$\sqrt{\frac{\sqrt{F_\beta}+\beta\lambda+\beta+\lambda}{6\beta\lambda}}$	0	$\sqrt{\frac{-\sqrt{F_\beta}+\beta(\lambda-1)+\lambda}{6\beta\lambda}}$
f_2	0	$\sqrt{\frac{-\sqrt{F_\beta}+\beta\lambda+\beta+\lambda}{6\beta\lambda}}$	0	$\sqrt{\frac{\sqrt{F_\beta}+\beta(\lambda-1)+\lambda}{6\beta\lambda}}$

$\Omega_{de}^{(m)} < 0.02$ (95% CL), at redshift de $z \approx 50$, according to CMB measurements [81], we get $-0.04 < \eta < 0$, which is also compatible with $0 < \Omega_m < 1$.

Additionally, the critical point i corresponds to a dark energy-dominated solution with a de Sitter EoS, where $w_{de} = w_{tot} = -1$. Consequently, this critical point results in accelerated expansion for all parameter values.

Finally, points i_1 and i_2 are not physically viable. For these points, the physical condition $0 < \Omega_m < 0$ implies $\eta < -3$ or $\eta > 6$, but this result is not compatible with a dark matter-dominated era as described by point h_M ($-0.04 < \eta < 0$). Hence, to reproduce the standard thermal history of the universe, we designate the points i_1 and i_2 as unphysical.

3.2 Stability of critical points

To study the stability of the critical points, we introduce time-dependent linear perturbations denoted as δx, δy, $\delta\varrho$, and δu around each critical point. These perturbations take the form of $x = x_c + \delta x$, $y = y_c + \delta y$, $\varrho = \varrho_c + \delta\varrho$, and $u = u_c + \delta u$. Substituting these expressions into the autonomous system (24) and linearizing the equations, we obtain the linear perturbation matrix $\mathcal{M}$, as outlined in [2]. The eigenvalues of $\mathcal{M}$, denoted as μ_1, μ_2, μ_3, and μ_4, evaluated at each fixed point, determine the stability conditions for those points. Typically, the classification of stability properties proceeds as follows: (i) A *stable node* exists when all the eigenvalues are negative, (ii) An *unstable node* emerges when all the eigenvalues are positive, (iii) A *saddle point* is characterized by having one, two, or three of the four eigenvalues as positive and the others as negative, (iv) A *stable spiral* is observed when the determinant of $\mathcal{M}$ is negative, and the real part of all the eigenvalues is negative. Points classified as stable nodes or stable spirals are referred to as *attractor points*, and these fixed points are reached during the cosmic evolution of the Universe, regardless of the initial conditions of the system, as long as they belong to the attraction basin of the critical point. In the following lines, we present the eigenvalues and stability conditions for each critical point in every interaction case.

3.2.1 Case I: $Q = 3\alpha H\rho_m$

- Point a_R has the eigenvalues

$$\mu_1 = 0,\ \mu_2 = -1,\ \mu_3 = 2,\ \mu_4 = 1-3\alpha, \tag{33}$$

  then this point is always unstable for all the values of α.
- Point b_M has the eigenvalues

$$\mu_1 = -1,\ \mu_2 = \frac{1}{2}(-1+3\alpha),\ \mu_3 = \frac{3}{2}(\alpha+1),\ \mu_4 = -1+3\alpha, \tag{34}$$

Table 4 Cosmological parameters for the critical points in Table 3

Name	Ω_{de}	Ω_m	Ω_r	w_{de}	w_{tot}
d_R	$3{u_c}^2$	0	$1-3{u_c}^2$	$\frac{1}{3}$	$\frac{1}{3}$
e_M	$\frac{3\beta}{1+3\beta}$	$\frac{1}{1+3\beta}$	0	$\frac{1}{3}$	$\sqrt{\frac{\beta}{1+3\beta}}$
f	1	0	0	-1	-1
f_1	$\frac{1}{\beta}+1$	$-\frac{1}{\beta}$	0	$-\frac{\beta}{\beta+1}$	-1
f_2	$\frac{1}{\beta}+1$	$-\frac{1}{\beta}$	0	$-\frac{\beta}{\beta+1}$	-1

Table 5 Critical points for the autonomous system. Where, $R_c=\sqrt{(2\eta(\lambda-3)-12\lambda)^2-72\eta(\eta+3)\lambda}$

Name	x_c	y_c	ϱ_c	u_c
g_R	0	0	$\sqrt{1-3{u_c}^2}$	u_c
h_M	0	0	0	$\sqrt{\frac{\eta}{9\eta-6}}$
i	0	$\frac{1}{\sqrt{3\lambda}}$	0	$\sqrt{\frac{\lambda-1}{3\lambda}}$
i_1	0	$\frac{1}{6}\sqrt{\frac{2\eta\lambda+6\eta-12\lambda+R_c}{\eta\lambda}}$	0	$\frac{1}{6}\sqrt{\frac{2\eta\lambda-6\eta-12\lambda-R_c}{\eta\lambda}}$
i_2	0	$\frac{1}{6}\sqrt{\frac{2\eta\lambda+6\eta-12\lambda-R_c}{\eta\lambda}}$	0	$\frac{1}{6}\sqrt{\frac{2\eta\lambda-6\eta-12\lambda+R_c}{\eta\lambda}}$

Table 6 Cosmological parameters for the critical points in Table 5

Name	Ω_{de}	Ω_m	Ω_r	w_{de}	w_{tot}
g_R	$3{u_c}^2$	0	$1-3{u_c}^2$	$\frac{1}{3}$	$\frac{1}{3}$
h_M	$\frac{\eta}{3\eta-2}$	$\frac{2(\eta-1)}{3\eta-2}$	0	$\frac{1}{3}$	$\frac{\eta}{9\eta-6}$
i	1	0	0	-1	-1
i_1	$\frac{1}{3}-\frac{2}{\eta}$	$\frac{2}{\eta}+\frac{2}{3}$	0	$\frac{3\eta}{6-\eta}$	-1
i_2	$\frac{1}{3}-\frac{2}{\eta}$	$\frac{2}{\eta}+\frac{2}{3}$	0	$\frac{3\eta}{6-\eta}$	-1

which is a saddle point when $\alpha>\frac{1}{3}$ or $-1<\alpha<\frac{1}{3}$. On the other hand, it becomes a stable node when $\alpha<-1$. However, this point cannot account for the current accelerated expansion of the Universe.

- Point c has the eigenvalues

$$\mu_1=-2,\ \mu_2=-3(\alpha+1),\\ \mu_{3,4}=\frac{-3\lambda\pm\sqrt{16\lambda-7\lambda^2}}{2\lambda}. \tag{35}$$

This is a de-Sitter solution, ensuring accelerated expansion for all parameter values. We observe that it is a stable node when $\alpha>-1$ and $1<\lambda\leq\frac{16}{7}$. Finally, this point never exhibits stable spiral behavior (Fig. 1).

3.2.2 Case II: $Q=3\beta H\frac{{\rho_m}^2}{\rho_m+\rho_{de}}$

- Point d_R has the eigenvalues

$$\mu_1=2,\ \mu_2=-1,\ \mu_3=1,\ \mu_4=0, \tag{36}$$

which tells us that it is always an unstable node.

- Point e_M has the eigenvalues

$$\mu_1=-\frac{1}{2(1+3\beta)},\ \mu_{2,3}=-1,\ \mu_4=\frac{3(1+4\beta)}{2(1+3\beta)}, \tag{37}$$

which is a saddle point when $\beta<-\frac{1}{3}$ or $\beta>-\frac{1}{4}$. On the other hand, it becomes a stable node when $-\frac{1}{3}<\beta<-\frac{1}{4}$. However, this point cannot account for the current accelerated expansion of the Universe.

- Point f has the eigenvalues

$$\mu_1=-2,\ \mu_2=-3,\ \mu_{3,4}=\frac{-3\pm\sqrt{-7+\frac{16}{\lambda}}}{2}. \tag{38}$$

This is a de-Sitter solution, hence ensuring accelerated expansion for all parameter values. We observe that it is a stable node when $1<\lambda\leq\frac{16}{7}$. Finally, this point never exhibits stable spiral behavior.

- Stability of points f_1 and f_2 is given by the solution of the characteristic polynomials (Fig. 2).

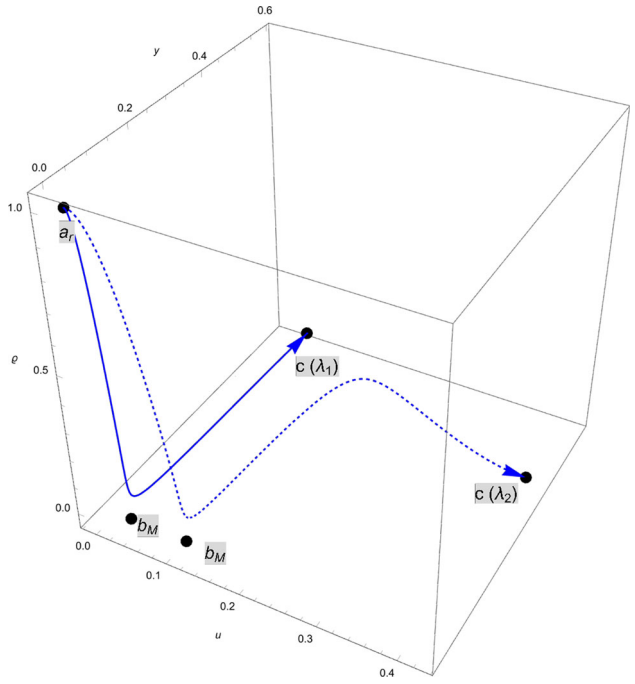

Fig. 1 Evolution curves in phase space for different values of λ and α. Blue solid lines correspond to initial conditions: $\alpha = 0.0014$, $\lambda = 1.004$, $x_i = 4 \times 10^{-9}$, $y_i = 4.9 \times 10^{-13}$, $\varrho_i = 0.99982$, and $u_i = 8 \times 10^{-5}$. Blue dashed lines correspond to initial conditions: $\alpha = 0.013$, $\lambda = 2.114$, $x_i = 8 \times 10^{-9}$, $y_i = 4.549 \times 10^{-13}$, $\varrho_i = 0.999708$, and $u_i = 5 \times 10^{-3}$. It is shown that both trajectories converge to the attractor c, which is a stable node that describes the dark-energy-dominated universe. Also, we have matched the current values for the fractional energy densities of dark energy $\Omega_{de}^{(0)} \approx 0.68$ and dark matter $\Omega_{dm}^{(0)} \approx 0.32$, at redshift $z = 0$, according to Planck results [82]

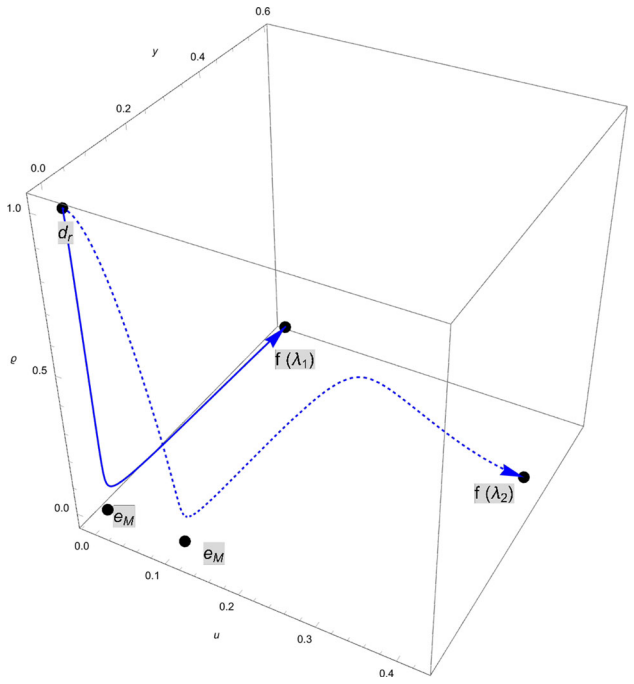

Fig. 2 Evolution curves in phase space for different values of λ and β. Blue solid lines correspond to initial conditions: $\beta = 0.00002$, $\lambda = 1.00004$, $x_i = 7.3 \times 10^{-8}$, $y_i = 5.02 \times 10^{-13}$, $\varrho_i = 0.999822$, and $u_i = 4 \times 10^{-8}$. Blue dashed lines correspond to initial conditions: $\beta = 0.014$, $\lambda = 2.09$, $x_i = 11.3 \times 10^{-7}$, $y_i = 4.36 \times 10^{-13}$, $\varrho_i = 0.999775$, and $u_i = 10^{-5}$. It is shown that both trajectories converge to the attractor f, which is a stable node that describes the dark-energy-dominated universe. Also, we have matched the current values for the fractional energy densities of dark energy $\Omega_{de}^{(0)} \approx 0.68$ and dark matter $\Omega_{dm}^{(0)} \approx 0.32$, at redshift $z = 0$, according to Planck results [82]

3.2.3 *Case III:* $Q = \dfrac{3}{2\kappa^2}\eta H^3(1 + \Omega_r - 3\Omega_{de})\Omega_m$

- Point g_R has the eigenvalues

$$\mu_1 = 0,\ \mu_2 = -1,\ \mu_3 = 2,\ \mu_4 = 1 + \eta - 6\eta {u_c}^2, \tag{39}$$

  which is always an unstable node.
- Point h_M has the eigenvalues

$$\mu_1 = -1,\ \mu_2 = \tfrac{1-\eta}{3\eta-2},\ \mu_3 = \tfrac{3-5\eta}{2-3\eta},\ \mu_4 = \eta - 1, \tag{40}$$

  which acts as a saddle point when $\frac{2}{3} < \eta < 1$, $\eta > 1$, or $\eta < \frac{3}{5}$. Conversely, it behaves as a stable node when $\frac{3}{5} < \eta < \frac{2}{3}$. Nonetheless, this point cannot explain the current accelerated expansion of the Universe.
- Point i has the eigenvalues

$$\mu_1 = -2,\ \mu_2 = -3 - \eta,\ \mu_{3,4} = \frac{-3 \pm \sqrt{-7 + \frac{16}{\lambda}}}{2}. \tag{41}$$

  This is a de-Sitter solution, ensuring accelerated expansion for all parameter values. We observe that it is a stable node when $\eta > -3$ and $1 < \lambda \leq \frac{16}{7}$. Finally, this point never exhibits stable spiral behavior.
- Stability of points i_1 and i_2 is given by the solution of the characteristic polynomials (Fig. 3).

A summary of this section is shown in Table 7, which contains the principal properties of critical points.

4 Numerical results

In this section, we aim to numerically solve the autonomous system represented by Eq. (24), associated with a set of cosmological equations (9)–(10). Our objective is to explore the characteristics of our model (for each interacting term Q) to explain the ongoing accelerated expansion of the Universe. Subsequently, we compare the predicted results with the most recent measurements of the Hubble parameter $H(z)$, Appendix A. We consider various parameter values and initial conditions with the aim of studying the behavior of cos-

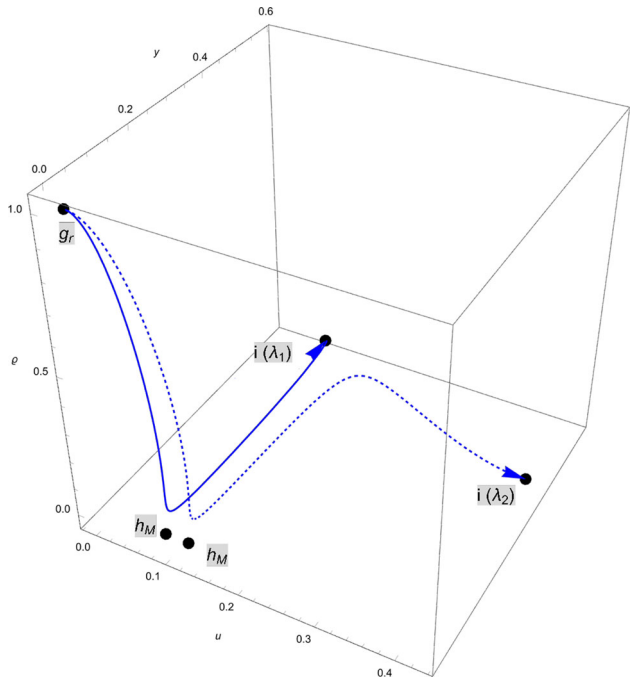

Fig. 3 Evolution curves in phase space for different values of λ and η. Blue solid lines correspond to initial conditions: $\eta = -0.05$, $\lambda = 1.01$, $x_i = 10^{-7}$, $y_i = 4.7 \times 10^{-13}$, $\varrho_i = 0.99974$, and $u_i = 10^{-7}$. Blue dashed lines correspond to initial conditions: $\eta = -0.1$, $\lambda = 2.2$, $x_i = 8 \times 10^{-6}$, $y_i = 4.3 \times 10^{-13}$, $\varrho_i = 0.99963$, and $u_i = 5 \times 10^{-3}$. It is shown that both trajectories converge to the attractor i, which is a stable node that describes the dark-energy-dominated universe. Also, we have matched the current values for the fractional energy densities of dark energy $\Omega_{de}^{(0)} \approx 0.68$ and dark matter $\Omega_{dm}^{(0)} \approx 0.32$, at redshift $z = 0$, according to Planck results [82]

mological parameters throughout the thermal history of the universe at intermediate redshifts. By investigating these several different parameter values and initial conditions, we can identify the range of potential evolutions for these cosmological parameters, all converging towards a common final-state attractor point.

4.1 Case I: $Q = 3\alpha H \rho_m$

We have presented the numerical results found for this interacting model in Figs. 1, 4, 5, 6 and 7.

In Fig. 1, we verify that the model provides a dark energy-dominated solution with attractor behavior. The attractor is a one-parameter solution, and thus, one can have different locations for this fixed point in the field space. This implies varying temporal durations for the transitions between the decelerating and accelerating phases. However, this is restricted by cosmological observations [82]. In Fig. 4, we depict the behavior of the energy density for radiation, matter, and dark energy. Remarkably, one can observe the scaling behavior of dark energy during the radiation and matter-dominated eras. This is an essential feature of the model because scaling solutions provide a natural mechanism to alleviate the energy scale problem of dark energy [41,83,84]. In Fig. 5, we show the evolution of both the EoS of dark energy and the total EoS.

Additionally, we added the corresponding curve associated with the ΛCDM model to contrast the predictions of our model. During the radiation and matter-dominated eras, the EoS of dark energy behaves like a radiation field, which is an expected result since the source of dark energy is a vector field [57]. Thus, in Fig. 6, we observe a slight discrepancy in the deceleration-acceleration transition redshift compared to the ΛCDM result. This latter result is validated in Fig. 7, where it shows the evolution of the Hubble rate $H(z)$ as a function of the redshift, along with the corresponding results from ΛCDM. In the same plot, we have depicted the relative difference for the ΛCDM model, showing that our results are compatible with observations (for more detail, see Table 8).

4.2 Case II: $Q = 3\beta H \dfrac{{\rho_m}^2}{\rho_m + \rho_{de}}$

For this ansatz, we have shown the numerical results in Figs. 2, 8, 9, 10 and 11.

In Fig. 2 one can see that the system has an attractor point, which is a dark energy-dominated solution. Furthermore, this attractor point has a nature of cosmological constant with an EoS $w_{de} = -1$. However, the position of this fixed point in the phase space depends on the parameter λ. Thus, the transition time between the dark matter-dominated era and late-time acceleration depends on it, too. Let us remember that this transition time is constrained by current cosmological observations [82]. In Fig. 8, we can observe the scaling regimes during the dark-matter and radiation-dominated epochs. At early times, the dark energy component reaches higher energy scales, alleviating the energy scale problem of dark energy. In Fig. 9, we depict the behavior of the EoS of dark energy and total EoS for our model, comparing the corresponding results from ΛCDM.

Interestingly enough, the evolution of the total EoS of our model is very close to that of ΛCDM, with some slight differences during the dark matter-dark energy transition time. However, the EoS of dark energy behaves like a radiation field at early times and like a cosmological constant at late times, also, in Fig. 10, one can observe the decelerating-accelerating transition time as described by the evolution of the deceleration parameter. We found that this transition time is slightly displaced towards smaller redshift values than the result from ΛCDM. Nevertheless, this result is still compatible with observational data [82].

Finally, in Fig. 11, we numerically corroborated that our model is compatible with observational data. The evolution of the Hubble rate is consistent with Hubble rate data found in the literature [85,86].

Table 7 Properties of the critical points

Cases	Name	Existence	Stability	Acceleration
	a_R	$\forall\,\lambda,\alpha$	Unstable $\forall\,\lambda,\alpha$	Never
I	b_M	$\alpha > 0$	Unstable for $\alpha > -1$	Never
	c	$\lambda > 1$	$\alpha > -1$ and $1 < \lambda \leq \frac{16}{7}$	Always
	d_R	$\forall\,\lambda,\beta$	Unstable $\forall\,\lambda,\beta$	Never
	e_M	$\beta < -\frac{1}{3} \vee \beta > 0$	Unstable for $\beta < -\frac{1}{3}$ or $\beta > -\frac{1}{4}$	Never
II	f	$\lambda > 1$	$1 < \lambda \leq \frac{16}{7}$	Always
	f_1	$\lambda > 1 \wedge 2\beta + \frac{\lambda(2\lambda+\sqrt{12\lambda-3}+1)}{(\lambda-1)^2} \leq 0$	Numerical solution only	Always
	f_2	$(\beta > 0 \wedge \lambda \neq 0) \vee \left(2\beta + \frac{\lambda(2\lambda+\sqrt{12\lambda-3}+1)}{(\lambda-1)^2} \leq 0 \wedge \lambda > 1\right)$	Numerical solution only	Always
	g_R	$\forall\,\lambda,\eta$	Unstable $\forall\,\lambda,\eta$	Never
	h_M	$\eta < 0 \vee \eta > \frac{2}{3}$	Unstable for $\eta < \frac{3}{5}$ and $\eta > \frac{2}{3}$	Never
	i	$\lambda > 1$	$\eta > -3$ and $1 < \lambda \leq \frac{16}{7}$	Always
		$(-3 < \eta < 0 \wedge (\lambda < 0 \vee 0 < \lambda \leq 1)) \vee \left(1 < \lambda < 3\left(\sqrt{15}+4\right) \wedge \frac{3(2\lambda^2+3\lambda)}{\lambda^2-24\lambda+9}\right.$		
	i_1	$\left.-9\sqrt{3}\sqrt{\frac{4\lambda^3-\lambda^2}{(\lambda^2-24\lambda+9)^2}} \leq \eta < 0\right) \vee$	Numerical solution only	Always
III		$\left(\eta < 0 \wedge \lambda = 3\left(\sqrt{15}+4\right)\right) \vee \left(\lambda > 3\left(\sqrt{15}+4\right) \wedge \left(\eta < 0 \vee \eta \geq \frac{3(2\lambda^2+3\lambda)}{\lambda^2-24\lambda+9} + 9\sqrt{3}\sqrt{\frac{4\lambda^3-\lambda^2}{(\lambda^2-24\lambda+9)^2}}\right)\right) \vee \left(1 < \lambda < 3\left(\sqrt{15}+4\right) \wedge \frac{3(2\lambda^2+3\lambda)}{\lambda^2-24\lambda+9}\right.$		
		$\left.-9\sqrt{3}\sqrt{\frac{4\lambda^3-\lambda^2}{(\lambda^2-24\lambda+9)^2}} \leq \eta < -3\right) \vee$		
	i_2	$\left(\eta < -3 \wedge \lambda = 3\left(\sqrt{15}+4\right)\right) \vee \left(\lambda > 3\left(\sqrt{15}+4\right) \wedge \left(\eta < -3 \vee \eta \geq \frac{3(2\lambda^2+3\lambda)}{\lambda^2-24\lambda+9} + 9\sqrt{3}\sqrt{\frac{4\lambda^3-\lambda^2}{(\lambda^2-24\lambda+9)^2}}\right)\right)$	Numerical solution only	Always

4.3 Case III: $Q = \frac{3}{2\kappa^2}\eta H^3(1+\Omega_r - 3\Omega_{de})\Omega_m$

Finally, for our third model, the numerical results are shown in Figs. 3, 12, 13, 14 and 15.

In Fig. 3, we show the evolution curves in the phase space for this ansatz. As for previous models, we have an attractor fixed point, which is a cosmological constant solution. This attractor solution with accelerated expansion has a variable position in the phase space, which depends on the model parameter related to the slope of the vector's potential. In Fig. 12, we show the scaling behavior for early times.

On the other hand, in Fig. 13 we depict the evolution of the EoS of dark energy and the total EoS. As before, the effective dark energy fluid behaves as radiation field density at early times, whereas it behaves as a quintessence field at late times, in Fig. 14, we observe that this model provides a deceleration-acceleration transition redshift closer to the value from the ΛCDM model, and therefore, it becomes compatible with observations [82]. This result is also corroborated in Fig. 15, where we plot the theoretical Hubble rate from our model along with the current Hubble rate data [85,86].

5 Thermodynamics

The Universe, as a whole, can be seen as a classical thermodynamic system composed of interacting fluids. The temperature is defined through the Gibbs equation

$$T d\left(\frac{S}{N}\right) = d\left(\frac{\rho}{n}\right) + p\left(\frac{1}{n}\right), \tag{42}$$

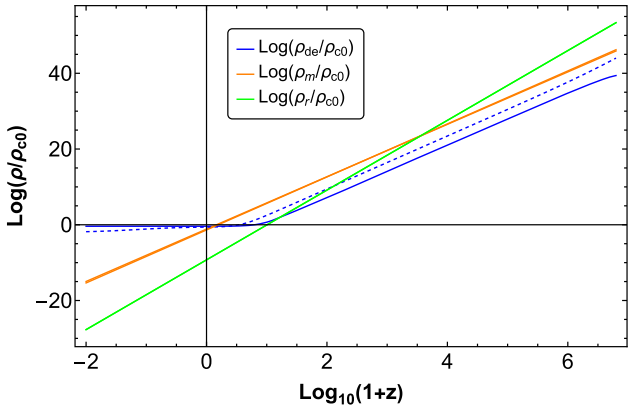

Fig. 4 We depict the evolution of the energy density of dark energy ($\rho_{\rm de}$) in blue, dark matter (including baryons) (ρ_m) in orange, and radiation (ρ_r) in green as functions of the redshift (z), for two values of λ and α. In particular, solid lines correspond to initial conditions: $\alpha = 0.0014$, $\lambda = 1.004$, $x_i = 4 \times 10^{-9}$, $y_i = 4.9 \times 10^{-13}$, $\varrho_i = 0.99982$, and $u_i = 8 \times 10^{-5}$. Dashed lines correspond to initial conditions: $\alpha = 0.013$, $\lambda = 2.114$, $x_i = 8\times10^{-9}$, $y_i = 4.549\times10^{-13}$, $\varrho_i = 0.999708$, and $u_i = 5 \times 10^{-3}$

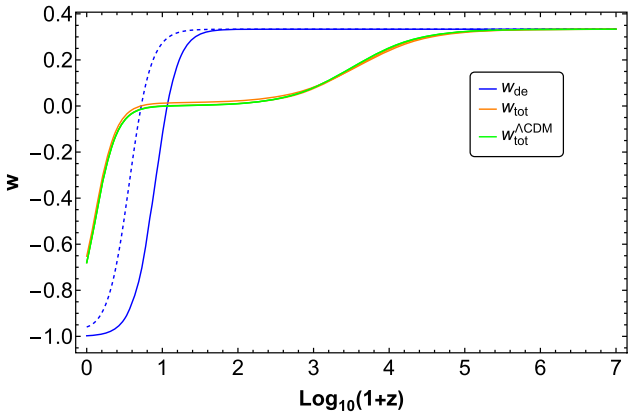

Fig. 5 We depict the total EoS parameter $w_{\rm tot}$ (orange line), the EOS parameter of dark energy $w_{\rm de}$ (blue line), and the total EOS of the ΛCDM model (green line) as redshift functions. We also used the same initial conditions as shown in Fig. 4 to obtain both the solid and dashed blue lines. For the dashed line, a value of $w_{\rm de} \approx -0.959$ is observed at the current time $z = 0$. Meanwhile, for the solid line, a value of $w_{\rm de} \approx -0.997$ is observed at the current time $z = 0$, which is consistent with the observational constraint $w_{\rm de}^{(0)} = -1.028 \pm 0.032$

where T is the temperature of the system and S is total entropy per comoving volume and $N = nV = const$ with $V = a^3$, and n is the number density.

This equation can be written as

$$T d\left(\frac{S}{N}\right) = d\left(\frac{d\rho}{nT}\right) - \left(\frac{\rho + p}{n^2 T}\right) dn. \tag{43}$$

Thus, the integrability condition

$$\frac{\partial^2 S}{\partial n \partial \rho} = \frac{\partial^2 S}{\partial \rho \partial n}, \tag{44}$$

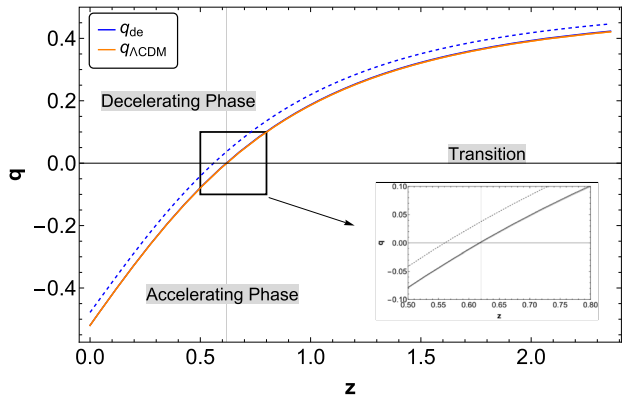

Fig. 6 We show the evolution of the deceleration parameter $q(z)$, for the same initial conditions used in Fig. 4

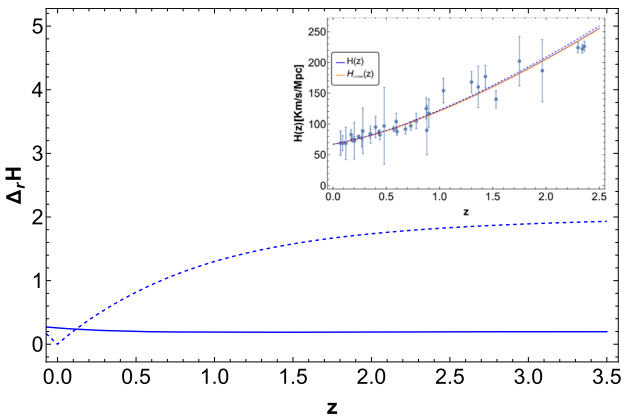

Fig. 7 We present the evolution of the Hubble rate $H(z)$ and its relative difference $\Delta_r H(z) = 100 \times |H - H_{\Lambda\rm CDM}|/H_{\Lambda\rm CDM}$ for the ΛCDM model, as functions of redshift, using the same initial conditions as shown in Fig. 4. This is complemented by the evolution of the Hubble rate $H_{\Lambda\rm CDM}$ in the ΛCDM model and the Hubble data from references [85,86]. We have employed the current value of the Hubble rate, $H_0 = 67.4$ km/(Mpc·s), from Planck 2018 [82]

can allow us to obtain

$$n\frac{\partial T}{\partial n} + (\rho + p)\frac{\partial T}{\partial \rho} = T\frac{\partial p}{\partial \rho}. \tag{45}$$

Since $T = T(n, \rho)$, and using the conservation laws

$$\dot{\rho} + 3H(\rho + p) = 0, \tag{46}$$

$$\dot{n} + 3Hn = 0, \tag{47}$$

where ρ and p are the total energy and pressure densities, we obtain

$$\dot{T} = -3H\left[\left(\frac{\partial T}{\partial n}\right)n + \left(\frac{\partial T}{\partial \rho}\right)(\rho + p)\right]. \tag{48}$$

Using the relation (45) we get

$$\frac{\dot{T}}{T} = -3H\left(\frac{\partial p}{\partial \rho}\right)_n. \tag{49}$$

Table 8 Hubble's parameter vs. redshift and scale factor

z	$H(z)$ ($\frac{\text{km/s}}{\text{Mpc}}$)	Refs.
0.07	69 ± 19.6	[98]
0.09	69 ± 12	[99]
0.100	69 ± 12	[99]
0.120	68.6 ± 26.2	[98]
0.170	83 ± 8	[99]
0.179	75 ± 4	[100]
0.199	75 ± 5	[100]
0.200	72.9 ± 29.6	[98]
0.270	77 ± 14	[99]
0.280	88.8 ± 36.6	[98]
0.320	79.2 ± 5.6	[101]
0.352	83 ± 14	[100]
0.3802	83 ± 13.5	[100]
0.400	95 ± 17	[99]
0.4004	77 ± 10.2	[100]
0.4247	87.1 ± 11.2	[100]
0.440	82.6 ± 7.8	[102]
0.4497	92.8 ± 12.9	[100]
0.470	89 ± 50	[103]
0.4783	80.9 ± 9	[100]
0.480	97 ± 62	[104]
0.570	100.3 ± 3.7	[101]
0.593	104 ± 13	[100]
0.600	87.9 ± 6.1	[102]
0.680	92 ± 8	[100]
0.730	97.3 ± 7	[102]
0.781	105 ± 12	[100]
0.875	125 ± 17	[100]
0.880	90 ± 40	[104]
0.900	117 ± 23	[99]
1.037	154 ± 20	[100]
1.300	168 ± 17	[99]
1.363	160 ± 33.6	[105]
1.430	177 ± 18	[99]
1.530	140 ± 14	[99]
1.750	202 ± 40	[99]
1.965	186.5 ± 50.4	[105]
2.340	222 ± 7	[106]
2.360	226 ± 8	[107]

In the case of a barotropic perfect fluid with pressure $p = w(a)\rho$ we obtain

$$T(a) = T(a_0) exp\left[-3\int_{a_0}^{a} da \frac{w(a)}{a}\right]. \tag{50}$$

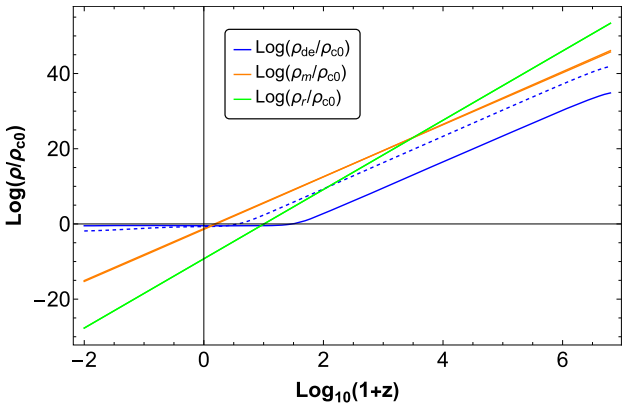

Fig. 8 We depict the evolution of the energy density of dark energy ρ_{de} (blue), dark matter (including baryons) ρ_m (orange), and radiation ρ_r (green) as functions of the redshift z, for two values of λ and β. In particular, solid lines correspond to initial conditions: $\beta = 0.00002$, $\lambda = 1.00004$, $x_i = 7.3 \times 10^{-8}$, $y_i = 5.02 \times 10^{-13}$, $\varrho_i = 0.999822$, and $u_i = 4 \times 10^{-8}$. Dashed lines correspond to initial conditions: $\beta = 0.014$, $\lambda = 2.09$, $x_i = 11.3 \times 10^{-7}$, $y_i = 4.36 \times 10^{-13}$, $\varrho_i = 0.999775$, and $u_i = 10^{-5}$

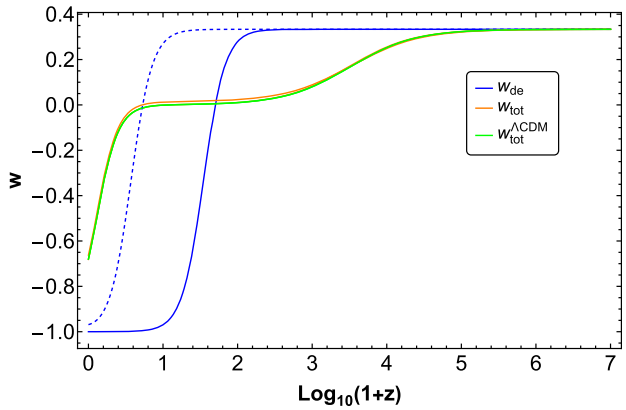

Fig. 9 We depict the total EoS parameter w_{tot} (orange line), the EOS parameter of dark energy w_{de} (blue line), and the total EOS of the ΛCDM model (green line) as redshift functions. We also used the same initial conditions as shown in Fig. 8 to obtain both the solid and dashed blue lines. For the dashed line, a value of $w_{\text{de}} \approx -0.968$ is observed at the current time $z = 0$. Meanwhile, for the solid line, a value of $w_{\text{de}} \approx -0.999$ is observed at the current time $z = 0$, which is consistent with the observational constraint $w_{\text{de}}^{(0)} = -1.028 \pm 0.032$

For two interacting fluids (dark matter and dark energy) one can write

$$\dot{\rho}_{de} + 3H(1 + w_{de}^{eff})\rho_{de} = 0, \tag{51}$$

$$\dot{\rho}_{m} + 3H(1 + w_{m}^{eff})\rho_{m} = 0, \tag{52}$$

where it has been defined

$$w_{de}^{eff} = w_{de} + \frac{Q}{3H\rho_{de}}, \tag{53}$$

$$w_{m}^{eff} = w_{m} - \frac{Q}{3H\rho_{m}}, \tag{54}$$

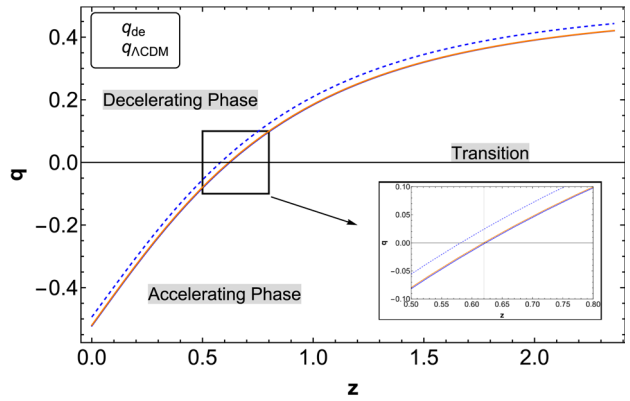

Fig. 10 We show the evolution of the deceleration parameter $q(z)$, for the same initial conditions used in Fig. 8

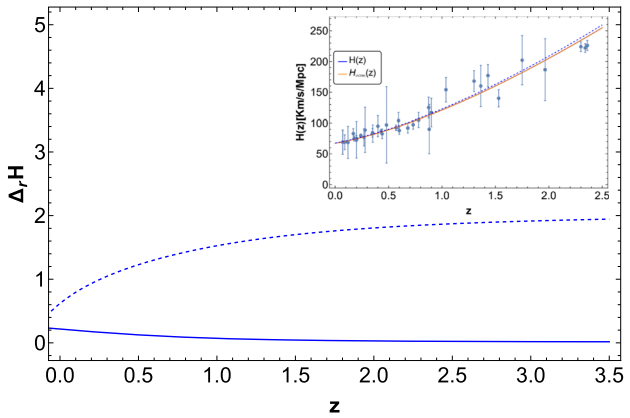

Fig. 11 We present the evolution of the Hubble rate $H(z)$ and its relative difference $\Delta_r H(z) = 100 \times |H - H_{\Lambda CDM}|/H_{\Lambda CDM}$ with respect to the ΛCDM model, as functions of redshift, using the same initial conditions as shown in Fig. 8. This is complemented by the evolution of the Hubble rate $H_{\Lambda CDM}$ in the ΛCDM model and the Hubble data from references [85,86]. We have employed the current value of the Hubble rate, $H_0 = 67.4$ km/(Mpc·s), from Planck 2018 [82]

and then Eq. (50) gives us

$$\frac{T_{de}(z)}{T_{de}(0)} = \exp\left[3\int_0^z d\ln(1+z) w_{de}^{eff}(z)\right], \tag{55}$$

$$\frac{T_m(z)}{T_m(0)} = (1+z)^{3w_m} \exp\left[-\int_0^z d\ln(1+z)\left(\frac{Q}{H\rho_m}\right)\right]. \tag{56}$$

Thus, one can verify that for non-relativistic matter $w_m = 0$, the temperature is constant in the absence of coupling. So, after specifying the coupling between dark matter and dark energy, we can evolve the temperature for both components as functions of redshifts. For the present interacting vector-like dark energy model, the time evolution of the effective EoS of dark energy w_{de}^{eff} depends on both the magnitude of the vector field and the coupling to matter. Therefore, temperature behavior is determined by the dynamics of the vector field. In Figs. 16, 17, and 18, we depict the temperature behavior of matter and dark energy, parameterized in terms of the ratios $T_{de}(z)/T_{de}^{(0)}$ and $T_m(z)/T_m^{(0)}$, respectively, as functions of redshift z for different initial conditions. Here, we define $T_m^{(0)} \equiv T_m(z=0)$ and $T_{de}^{(0)} \equiv T_{de}(z=0)$. Also, in Fig. 19, we depict the behavior of the coupling function $Q(z)$ for the three models studied. From Figs. 16, 17, and 18, it is evident that the temperature of matter increases very slowly, while the temperature of dark energy rises more rapidly. Consequently, when we combine these findings with Fig. 19, we observe an energy transference from dark energy to dark matter, indicating that dark energy possesses a negative heat capacity. Furthermore, it is verified that the second law of thermodynamics

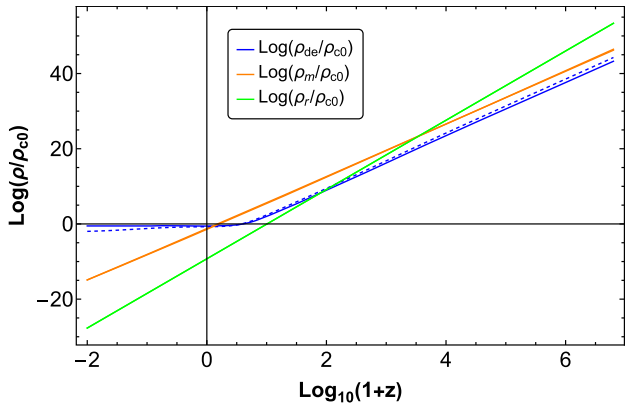

Fig. 12 We depict the evolution of the energy density of dark energy ρ_{de} (blue), dark matter (including baryons) ρ_m (orange), and radiation ρ_r (green) as functions of the redshift z, for two values of λ and β. In particular, solid lines correspond to initial conditions: $\eta = -0.05$, $\lambda = 1.01$, $x_i = 10^{-7}$, $y_i = 4.7\times10^{-13}$, $\varrho_i = 0.99974$, and $u_i = 10^{-7}$. Dashed lines correspond to initial conditions: $\eta = -0.1$, $\lambda = 2.2$, $x_i = 8\times10^{-6}$, $y_i = 4.3\times10^{-13}$, $\varrho_i = 0.99963$, and $u_i = 5\times10^{-3}$

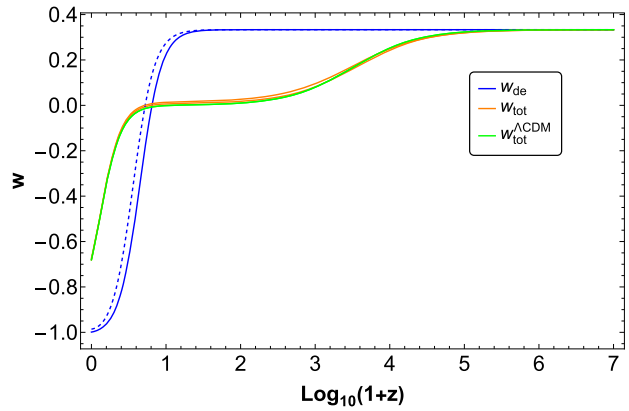

Fig. 13 We depict the total EoS parameter w_{tot} (orange line), the EOS parameter of dark energy w_{de} (blue line), and the total EOS of the ΛCDM model (green line) as redshift functions. We also used the same initial conditions as shown in Fig. 12 to obtain both the solid and dashed blue lines. For the dashed line, a value of $w_{de} \approx -0.986$ is observed at the current time $z = 0$. Meanwhile, for the solid line, a value of $w_{de} \approx -0.999$ is observed at the current time $z = 0$, which is consistent with the observational constraint $w_{de}^{(0)} = -1.028 \pm 0.032$

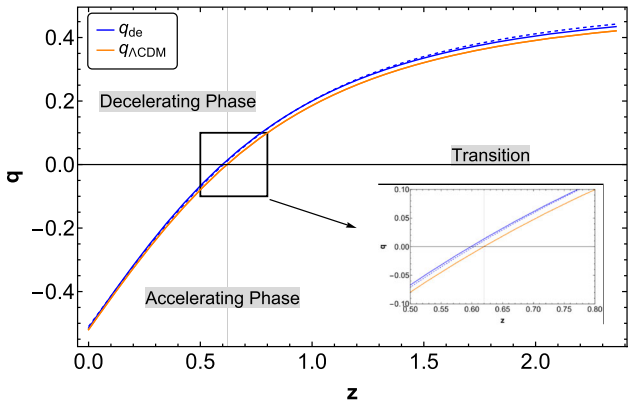

Fig. 14 We show the evolution of the deceleration parameter $q(z)$, for the same initial conditions used in Fig. 12

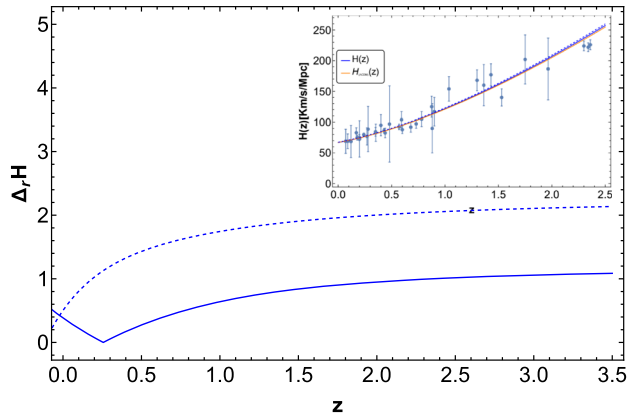

Fig. 15 We present the evolution of the Hubble rate $H(z)$ and its relative difference $\Delta_r H(z) = 100 \times |H - H_{\Lambda CDM}|/H_{\Lambda CDM}$ with respect to the ΛCDM model, as functions of redshift, using the same initial conditions as shown in Fig. 12. This is complemented by the evolution of the Hubble rate $H_{\Lambda CDM}$ in the ΛCDM model and the Hubble data from references [85,86]. We have employed the current value of the Hubble rate, $H_0 = 67.4$ km/(Mpc·s), from Planck 2018 [82]

is satisfied during the regime $T_m < T_{de}$ for $Q > 0$. From the Gibbs equation (42) and the continuity equations (19) and (20) one can demonstrate that $T_{de}dS_{de} = -QVdt$ and $T_m dS_m = QVdt$, where S_m and S_{de} represent the entropy of matter and dark energy, respectively. Consequently, we can verify that $d(S_{de} + S_m) = dS_{tot} = QV(1/T_m - 1/T_{de})dt$, and the second law $d(S_{de} + S_m) > 0$, requires $T_m < T_{de}$ if $Q > 0$, or $T_m > T_{de}$ if $Q < 0$ [87]. In Figs. 16, 17, and 18, we observe that $T_{de}(z)/T_{de}^{(0)} < T_m(z)/T_m^{(0)}$. Thus, for $Q > 0$, the validity of the second law requires $T_m < T_{de}$ [87], and therefore $T_m^{(0)} < T_{de}^{(0)}$ (see Appendix B).

In the case of model III, we observe a sign change in Q, which suggests a change in the direction of the energy flux. This could imply a corresponding sign change in the heat capacity of dark energy, which must be in concordance with the temperature behavior in Fig. 18 (see Refs. [87,88]).

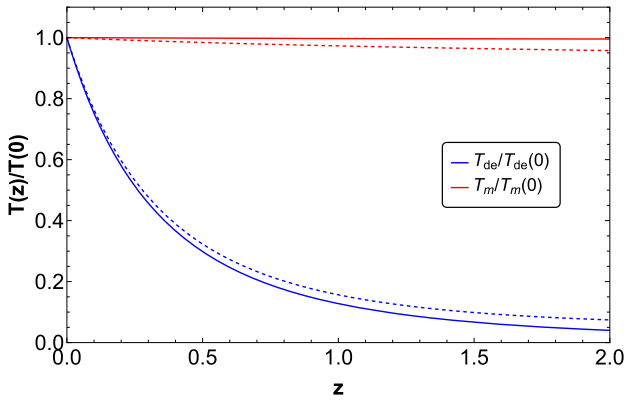

Fig. 16 We depict the evolution of the temperature of dark energy and dark matter as a function of the redshift for interaction "Case I" using the same set of initial conditions used in Fig. 4

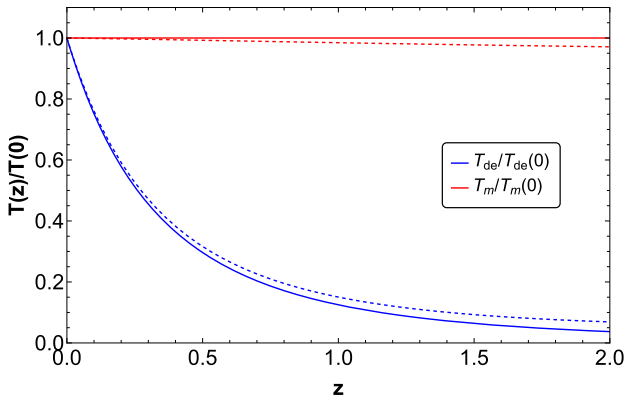

Fig. 17 We depict the evolution of the temperature of dark energy and dark matter as a function of the redshift for interaction "Case II" using the same set of initial conditions used in Fig. 8

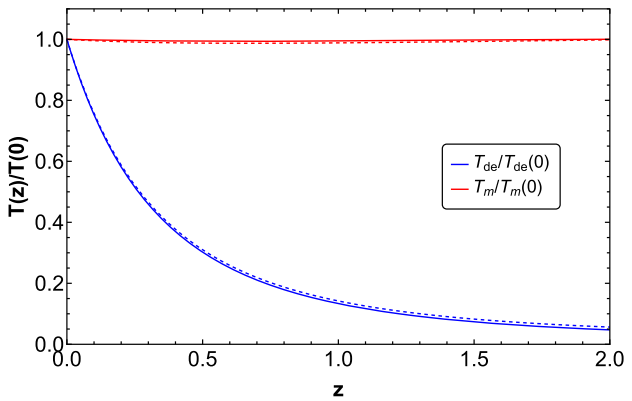

Fig. 18 We depict the evolution of the temperature of dark energy and dark matter as a function of the redshift for interaction "Case III" using the same set of initial conditions used in Fig. 12

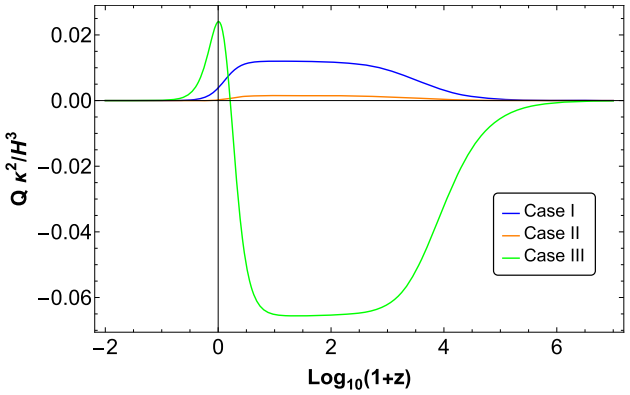

Fig. 19 We depict the evolution of the interaction term Q for each case considered

6 Concluding remarks

In the present paper, we studied the cosmological dynamics of interacting vector-like dark energy. The vector-like dark energy refers to the "cosmic triad", which consists of three identical vectors oriented in mutually orthogonal directions and thus preserving the space isotropy [57]. Furthermore, we assumed an interaction between dark energy and dark matter. This interaction is described by the function Q, which is a function of the energy densities of both dark energy and dark matter, as well as the Hubble rate. Thus, we have studied several different models for Q [76].

We have shown that the cosmic triad can explain the dynamics of dark energy, providing a dark energy-dominated solution with accelerated expansion. These dark energy solutions are attractors fixed points, and thus, the system will reach them over a wide range of initial conditions. Nevertheless, one can observe that the whole cosmological evolution is altered by the presence of interaction between the effective dark energy fluid and dark matter. In particular, we obtained new scaling solutions of radiation and dark matter, which originate from both the pure dynamics of the vector field and the matter-vector interaction function Q.

It is important to note that although the critical point describing the dark energy-dominated era is an attractor, reachable through a wide set of initial conditions, fine-tuning is still required. This is to ensure consistency with the current estimations of cosmological parameters at redshift $z = 0$, as well as to accurately reproduce the thermal history of the universe in line with observational data. The need for fine-tuning arises because the attractor critical point is only asymptotically achieved in the future, not precisely at $z = 0$. To address this issue of finite-tuning, also known as the cosmological coincidence problem [2], the existence of an attractor scaling solution featuring accelerated expansion may be necessary. However, obtaining such solutions is inherently difficult. Not all dark energy models offer this kind of solution [19,89,90], and in some cases, even when these solutions are present, the model may not successfully replicate the dark matter era [91].

As the scaling solutions contribute to the existence of small amounts of dark energy in the radiation and matter era, they can give rise to notable physical outcomes [83,84]. This specifically changes the Hubble rate during that era, leading to adjustments in the theoretical forecasts for the abundances of primordial light elements [79,80]. Furthermore, the shape of the Cosmic Microwave Background (CMB) anisotropies spectrum is profoundly affected by such a scaling field [80]. The influence of this scaling field also extends to the development of the universe's large-scale structures, affecting the evolution of cosmic entities like galaxies and galaxy clusters [91].

We also have studied the thermodynamics of our model, considering the interaction function Q. Using the Gibbs equation applied to an expanding universe, one can obtain general expressions for the temperature of dark matter and dark energy as functions of redshift in the presence of interaction between them [87]. We have analyzed three types of interaction functions Q that depend on the energy density of dark energy and dark matter. Since the effective dark energy depends on the vector field and its dynamics, the interaction function Q does well. In particular, we found for each interaction model the expressions for Q in terms of the dynamical variables. By numerically solving the background equations and using the expressions for Q in terms of the phase-space variables, we have depicted the behavior of the temperatures of dark energy and dark matter. Our results showed us that the temperature of matter increases very slowly, whereas the temperature of dark energy rises more quickly. Thus, we corroborated that there is a transference of energy from dark energy to dark matter, as dark energy has a negative heat capacity. In this way, we verified that the second law of thermodynamics is satisfied during the regime $T_m < T_{de}$ for $Q > 0$ [87], provided that $T_m^{(0)} < T_{de}^{(0)}$ However, it is important to note that measuring the temperature of dark matter and dark energy is extremely challenging [87,92,93]. Currently, the temperatures of these components remain unknown. Additionally, developing a suitable thermodynamic framework for the dark energy sector continues to be an area of active research due to the existing gaps in our understanding of its intrinsic nature. It is conceivable that future astronomical and cosmological observations will enhance our understanding of these elusive components , thereby enriching our knowledge of their thermodynamic evolution [94,95]. The analysis of the models studied through the interaction term (as shown in Fig. 19) determines that the models include a change of sign for the dark energy interaction function. Since the interaction terms change their signs during evolution, our results indicate that today, dark energy is transferred to dark matter, but in the past, the transfer was the opposite [78,96,97].

Acknowledgements M. Gonzalez-Espinoza acknowledges the financial support of FONDECYT de Postdoctorado, N° 3230801. G. Otalora acknowledges Dirección de Investigación, Postgrado y Transferencia Tecnológica de la Universidad de Tarapacá for financial support through Proyecto UTA Mayor 4731-23. C. Rodriguez-Benites and M. Alva-Morales acknowledge the financial support of PE501082885-2023-PROCIENCIA.

Data Availability Statement This manuscript has no associated data or the data will not be deposited. [Authors' comment: The present work is a theoretical study, and therefore no experimental data has been listed.]

Code availability My manuscript has no associated code/software. [Author's comment: The present work is a theoretical study, and no associated code/software is involved.]

Funded by SCOAP[3].

Appendix A: Hubble's parameter data

In this appendix, we present Hubble's parameter data for $0.01 < z < 2.360$:

Appendix B: Thermodynamics calculations

From Figs. 16, 17, and 18 we see that

$$\frac{T_{de}}{T_{de}^{(0)}} < \frac{T_m}{T_m^{(0)}}, \tag{B1}$$

where $T_{de}^{(0)} = T_{de}(z=0)$ and $T_m^{(0)} = T_m(z=0)$. Then, from (B1) we obtain

$$T_{de} < T_m \frac{T_{de}^{(0)}}{T_m^{(0)}}. \tag{B2}$$

We know that for $Q > 0$, the second law of thermodynamics requires $T_m < T_{de}$ [87]. Therefore, we have:

$$T_m < T_{de} < T_m \frac{T_{de}^{(0)}}{T_m^{(0)}}. \tag{B3}$$

Consequently, we get

$$T_m < T_m \frac{T_{de}^{(0)}}{T_m^{(0)}} \Rightarrow T_m^{(0)} < T_{de}^{(0)}. \tag{B4}$$

References

1. P.A. Ade, N. Aghanim, M. Arnaud, M. Ashdown, J. Aumont, C. Baccigalupi, A. Banday, R. Barreiro, J. Bartlett, N. Bartolo et al., Planck 2015 results-xiii. Cosmological parameters. Astron. Astrophys. **594**, A13 (2016)
2. E.J. Copeland, M. Sami, S. Tsujikawa, Dynamics of dark energy. Int. J. Mod. Phys. D **15**, 1753 (2006). arXiv:hep-th/0603057
3. S.M. Carroll, The cosmological constant. Living Rev. Relativ. **4**, 1 (2001). arXiv:astro-ph/0004075
4. A. Padilla, *Lectures on the Cosmological Constant Problem* (2015). arXiv:1502.05296 [hep-th]
5. C. Wetterich, The cosmological constant and the time variation of the fundamental constants. Astron. Astrophys. **301**, 321 (2015)
6. S. Tsujikawa, Modified gravity models of dark energy. Lect. Notes Phys. **800**, 99 (2010). arXiv:1101.0191 [gr-qc]
7. S. Nojiri, S.D. Odintsov, Introduction to modified gravity and gravitational alternative for dark energy. eConf **C0602061**, 06 (2006). arXiv:hep-th/0601213
8. S. Weinberg, The cosmological constant problem. Rev. Mod. Phys. **61**, 1 (1989)
9. J. Martin, Everything you always wanted to know about the cosmological constant problem (but were afraid to ask). Comptes Rendus Phys. **13**, 566 (2012). arXiv:1205.3365 [astro-ph.CO]
10. E. Abdalla et al., Cosmology intertwined: a review of the particle physics, astrophysics, and cosmology associated with the cosmological tensions and anomalies, in *2022 Snowmass Summer Study* JHEAp **34**, 49–211 (2022). arXiv:2203.06142 [astro-ph.CO]. https://doi.org/10.1016/j.jheap.2022.04.002
11. E. Di Valentino et al., Snowmass 2021—letter of interest cosmology intertwined II: the Hubble constant tension. Astropart. Phys. **131**, 102605 (2021). arXiv:2008.11284 [astro-ph.CO]
12. E. Di Valentino et al., Cosmology intertwined III: $f\sigma_8$ and S_8. Astropart. Phys. **131**, 102604 (2021). arXiv:2008.11285 [astro-ph.CO]
13. L. Heisenberg, H. Villarrubia-Rojo, J. Zosso, Simultaneously solving the H0 and $\sigma 8$ tensions with late dark energy. Phys. Dark Universe **39**, 101163 (2023). arXiv:2201.11623 [astro-ph.CO]
14. A.G. Riess, The expansion of the universe is faster than expected. Nat. Rev. Phys. **2**, 10 (2019). arXiv:2001.03624 [astro-ph.CO]
15. C. Heymans et al., KiDS-1000 cosmology: multi-probe weak gravitational lensing and spectroscopic galaxy clustering constraints. Astron. Astrophys. **646**, A140 (2021). arXiv:2007.15632 [astro-ph.CO]
16. R.C. Nunes, S. Vagnozzi, Arbitrating the S8 discrepancy with growth rate measurements from redshift-space distortions. Mon. Not. R. Astron. Soc. **505**, 5427 (2021). arXiv:2106.01208 [astro-ph.CO]
17. L. Heisenberg, H. Villarrubia-Rojo, J. Zosso, Can late-time extensions solve the H0 and $\sigma 8$ tensions? Phys. Rev. D **106**, 043503 (2022). arXiv:2202.01202 [astro-ph.CO]
18. U. Kasper, On the cosmological constant problem and inflation in the framework of nonminimal coupling. Nuovo Cim. B **103**, 291 (1989)
19. L. Amendola, Scaling solutions in general nonminimal coupling theories. Phys. Rev. D **60**, 043501 (1999). arXiv:astro-ph/9904120
20. J.-P. Uzan, Cosmological scaling solutions of nonminimally coupled scalar fields. Phys. Rev. D **59**, 123510 (1999). arXiv:gr-qc/9903004
21. T. Chiba, Quintessence, the gravitational constant, and gravity. Phys. Rev. D **60**, 083508 (1999). arXiv:gr-qc/9903094
22. N. Bartolo, M. Pietroni, Scalar tensor gravity and quintessence. Phys. Rev. D **61**, 023518 (2000). arXiv:hep-ph/9908521

23. F. Perrotta, C. Baccigalupi, S. Matarrese, Extended quintessence. Phys. Rev. D **61**, 023507 (1999). arXiv:astro-ph/9906066
24. R. Gannouji, D. Polarski, A. Ranquet, A.A. Starobinsky, Scalar–tensor models of normal and phantom dark energy. JCAP. **09**, 016 (2006). arXiv:astro-ph/0606287
25. Z. Davari, V. Marra, M. Malekjani, Cosmological constrains on minimally and non-minimally coupled scalar field models. Mon. Not. R. Astron. Soc. **491**, 1920 (2020). arXiv:1911.00209 [gr-qc]
26. J.R. Ellis, S. Kalara, K.A. Olive, C. Wetterich, Density dependent couplings and astrophysical bounds on light scalar particles. Phys. Lett. B **228**, 264 (1989)
27. C. Wetterich, The Cosmon model for an asymptotically vanishing time dependent cosmological 'constant'. Astron. Astrophys. **301**, 321 (1995). arXiv:hep-th/9408025
28. T. Damour, K. Nordtvedt, Tensor–scalar cosmological models and their relaxation toward general relativity. Phys. Rev. D **48**, 3436 (1993)
29. L. Amendola, Coupled quintessence. Phys. Rev. D **62**, 043511 (2000)
30. E. Di Valentino, A. Melchiorri, O. Mena, S. Vagnozzi, Interacting dark energy in the early 2020s: a promising solution to the H_0 and cosmic shear tensions. Phys. Dark Universe **30**, 100666 (2020). arXiv:1908.04281 [astro-ph.CO]
31. E. Di Valentino, A. Melchiorri, O. Mena, S. Vagnozzi, Nonminimal dark sector physics and cosmological tensions. Phys. Rev. D **101**, 063502 (2020). arXiv:1910.09853 [astro-ph.CO]
32. S. Tsujikawa, Matter density perturbations and effective gravitational constant in modified gravity models of dark energy. Phys. Rev. D **76**, 023514 (2007). arXiv:0705.1032 [astro-ph]
33. A. De Felice, S. Mukohyama, S. Tsujikawa, Density perturbations in general modified gravitational theories. Phys. Rev. D **82**, 023524 (2010). arXiv:1006.0281 [astro-ph.CO]
34. V. Faraoni, *Cosmology in Scalar Tensor Gravity* (Springer, Berlin, 2004)
35. H. Farajollahi, M. Setare, F. Milani, F. Tayebi, Cosmic dynamics in $F(R,\phi)$ gravity. Gen. Relativ. Gravit. **43**, 1657 (2011). arXiv:1005.2026 [physics.gen-ph]
36. F. Hammad, Density perturbations in f(R,ϕ) gravity with an application to the varying-power-law model. Phys. Rev. D **96**, 064006 (2017). arXiv:1709.02276 [gr-qc]
37. J. Solà Peracaula, A. Gomez-Valent, J. de Cruz Pérez, C. Moreno-Pulido, Brans–Dicke gravity with a cosmological constant smoothes out ΛCDM tensions. Astrophys. J. Lett. **886**, L6 (2019). arXiv:1909.02554 [astro-ph.CO]
38. J. Solà Peracaula, A. Gómez-Valent, J. de Cruz Pérez, C. Moreno-Pulido, Brans–Dicke cosmology with a Λ-term: a possible solution to ΛCDM tensions. Class. Quantum Gravity **37**, 245003 (2020). arXiv:2006.04273 [astro-ph.CO]
39. M. Hohmann, L. Järv, U. Ualikhanova, Covariant formulation of scalar-torsion gravity. Phys. Rev. D **97**, 104011 (2018). arXiv:1801.05786 [gr-qc]
40. M. Gonzalez-Espinoza, G. Otalora, Generating primordial fluctuations from modified teleparallel gravity with local Lorentz-symmetry breaking. Phys. Lett. B **809**, 135696 (2020). arXiv:2005.03753 [gr-qc]
41. M. Gonzalez-Espinoza, G. Otalora, Cosmological dynamics of dark energy in scalar-torsion $f(T,\phi)$ gravity. Eur. Phys. J. C **81**, 480 (2021). arXiv:2011.08377 [gr-qc]
42. M. Gonzalez-Espinoza, G. Otalora, J. Saavedra, Stability of scalar perturbations in scalar-torsion $f(T,\phi)$ gravity theories in the presence of a matter fluid. JCAP. **10**, 007 (2021). arXiv:2101.09123 [gr-qc]
43. M. Gonzalez-Espinoza, R. Herrera, G. Otalora, J. Saavedra, Reconstructing inflation in scalar-torsion $f(T,\phi)$ gravity. Eur. Phys. J. C **81**, 731 (2021). arXiv:2106.06145 [gr-qc]
44. L.K. Duchaniya, B. Mishra, J. Levi Said, Noether symmetry approach in scalar-torsion $f(T,\phi)$ gravity. Eur. Phys. J. C **83**, 613 (2023). arXiv:2210.11944 [gr-qc]
45. L.K. Duchaniya, S.A. Kadam, J. Levi Said, B. Mishra, Dynamical systems analysis in $f(T,\phi)$ gravity. Eur. Phys. J. C **83**, 27 (2023). arXiv:2209.03414 [gr-qc]
46. M. Gonzalez-Espinoza, G. Otalora, Y. Leyva, J. Saavedra, Phase-space analysis of torsion-coupled dilatonic ghost condensate (2023). arXiv preprint. arXiv:2306.03386 [gr-qc]
47. Y.-F. Cai, S. Capozziello, M. De Laurentis, E.N. Saridakis, f(T) teleparallel gravity and cosmology. Rep. Prog. Phys. **79**, 106901 (2016). arXiv:1511.07586 [gr-qc]
48. A. De Felice, L. Heisenberg, R. Kase, S. Mukohyama, S. Tsujikawa, Y.-L. Zhang, Cosmology in generalized Proca theories. JCAP **06**, 048 (2016). arXiv:1603.05806 [gr-qc]
49. A. De Felice, L. Heisenberg, R. Kase, S. Mukohyama, S. Tsujikawa, Y.-L. Zhang, Effective gravitational couplings for cosmological perturbations in generalized Proca theories. Phys. Rev. D **94**, 044024 (2016). arXiv:1605.05066 [gr-qc]
50. S. Nakamura, R. Kase, S. Tsujikawa, Coupled vector dark energy. JCAP. **12**, 032 (2019). arXiv:1907.12216 [gr-qc]
51. A. De Felice, S. Nakamura, S. Tsujikawa, Suppressed cosmic growth in coupled vector–tensor theories. Phys. Rev. D **102**, 063531 (2020). arXiv:2004.09384 [gr-qc]
52. W. Cardona, J.L. Palacios-Córdoba, C.A. Valenzuela-Toledo, Scrutinizing coupled vector dark energy in light of data (2023). arXiv preprint. arXiv:2310.13877 [astro-ph.CO]
53. J.B. Orjuela-Quintana, C.A. Valenzuela-Toledo, Anisotropic k-essence. Phys. Dark Universe **33**, 100857 (2021). arXiv:2106.06432 [gr-qc]
54. T. Koivisto, D.F. Mota, Vector field models of inflation and dark energy. JCAP **08**, 021 (2008). arXiv:0805.4229 [astro-ph]
55. L.H. Ford, Inflation driven by a vector field. Phys. Rev. D **40**, 967 (1989)
56. A.B. Burd, J.E. Lidsey, An analysis of inflationary models driven by vector fields. Nucl. Phys. B **351**, 679 (1991)
57. C. Armendariz-Picon, Could dark energy be vector-like? JCAP **07**, 007 (2004). arXiv:astro-ph/0405267
58. L.G. Gomez, Y. Rodriguez, Coupled multi-Proca vector dark energy. Phys. Dark Universe **31**, 100759 (2021). arXiv:2004.06466 [gr-qc]
59. M. Gonzalez-Espinoza, G. Otalora, Y. Leyva, J. Saavedra, Dynamics of dark energy in a scalar–vector-torsion theory. Eur. Phys. J. Plus **138**, 600 (2023). arXiv:2212.12071 [gr-qc]
60. Y. Rodríguez, A.A. Navarro, Non-abelian S-term dark energy and inflation. Phys. Dark Universe **19**, 129 (2018). arXiv:1711.01935 [gr-qc]
61. J.C. Garnica, L.G. Gomez, A.A. Navarro, Y. Rodriguez, Constant-roll inflation in the generalized SU(2) Proca theory. Ann. Phys. **534**, 2100453 (2022). arXiv:2109.10154 [gr-qc]
62. A. Golovnev, V. Mukhanov, V. Vanchurin, Vector inflation. JCAP **06**, 009 (2008). arXiv:0802.2068 [astro-ph]
63. G. Otalora, A. Övgün, J. Saavedra, N. Videla, Inflation from a nonlinear magnetic monopole field nonminimally coupled to curvature. JCAP **06**, 003 (2018). arXiv:1803.11358 [gr-qc]
64. T.S. Koivisto, N.J. Nunes, Inflation and dark energy from three-forms. Phys. Rev. D **80**, 103509 (2009). arXiv:0908.0920 [astro-ph.CO]
65. R.C.G. Landim, Dynamical analysis for a vector-like dark energy. Eur. Phys. J. C **76**, 480 (2016). arXiv:1605.03550 [hep-th]
66. Y. Zhang, Y.-G. Gong, Z.-H. Zhu, Noether symmetry approach in 'cosmic triad' vector field scenario. Class. Quantum Gravity **27**, 135019 (2010). arXiv:0912.4766 [astro-ph.CO]
67. Y. Zhang, Y. Gong, Z.-H. Zhu, The unified first law in "cosmic triad" vector field scenario. Phys. Lett. B **700**, 254 (2011). arXiv:1108.1046 [hep-th]

68. H. Wei, R.-G. Cai, Interacting vector-like dark energy, the first and second cosmological coincidence problems. Phys. Rev. D **73**, 083002 (2006). arXiv:astro-ph/0603052
69. H. Wei, S.N. Zhang, Observational H(z) data and cosmological models. Phys. Lett. B **644**, 7 (2007). arXiv:astro-ph/0609597
70. C. Wetterich, Phenomenological parameterization of quintessence. Phys. Lett. B **594**, 17 (2004)
71. L.P. Chimento, A.S. Jakubi, D. Pavon, W. Zimdahl, Interacting quintessence solution to the coincidence problem. Phys. Rev. D **67**, 083513 (2003)
72. C.G. Boehmer, G. Caldera-Cabral, R. Lazkoz, R. Maartens, Dynamics of dark energy with a coupling to dark matter. Phys. Rev. D **78**, 023505 (2008)
73. A.A. Costa et al., Constraints on interacting vector-like dark energy from cosmological observations. JCAP **12**, 050 (2021)
74. A. Morandi, M. Sun, Probing dark energy via galaxy cluster outskirts. Mon. Not. R. Astron. Soc. **457**, 3266 (2016). arXiv:1601.03741 [astro-ph.CO]
75. A.A. Costa, X.-D. Xu, B. Wang, E. Abdalla, Constraints on interacting dark energy models from Planck 2015 and redshift-space distortion data. JCAP **01**, 028 (2017). arXiv:1605.04138 [astro-ph.CO]
76. B. Wang, E. Abdalla, F. Atrio-Barandela, D. Pavon, Dark matter and dark energy interactions: theoretical challenges, cosmological implications and observational signatures. Rep. Prog. Phys. **79**, 096901 (2016). arXiv:1603.08299 [astro-ph.CO]
77. S. Lepe, G. Otalora, J. Saavedra, Dynamics of viscous cosmologies in the full Israel–Stewart formalism. Phys. Rev. D **96**, 023536 (2017). arXiv:1704.05625 [gr-qc]
78. F. Arévalo, A. Cid, Dynamics and statefinder analysis of a class of sign-changeable interacting dark energy scenarios. Eur. Phys. J. C **82**, 946 (2022)
79. P.G. Ferreira, M. Joyce, Cosmology with a primordial scaling field. Phys. Rev. D **58**, 023503 (1998). arXiv:astro-ph/9711102
80. R. Bean, S.H. Hansen, A. Melchiorri, Early universe constraints on a primordial scaling field. Phys. Rev. D **64**, 103508 (2001). arXiv:astro-ph/0104162
81. P. Ade et al. (Planck), Planck 2015 results. XIV. Dark energy and modified gravity. Astron. Astrophys. **594**, A14 (2016). arXiv:1502.01590 [astro-ph.CO]
82. N. Aghanim et al. (Planck), Planck 2018 results. VI. Cosmological parameters. Astron. Astrophys. **641**, A6 (2020). arXiv:1807.06209 [astro-ph.CO]
83. I.S. Albuquerque, N. Frusciante, N.J. Nunes, S. Tsujikawa, New scaling solutions in cubic Horndeski theories. Phys. Rev. D **98**, 064038 (2018). arXiv:1807.09800 [gr-qc]
84. J. Ohashi, S. Tsujikawa, Assisted dark energy. Phys. Rev. D **80**, 103513 (2009). arXiv:0909.3924 [gr-qc]
85. S.-L. Cao, X.-W. Duan, X.-L. Meng, T.-J. Zhang, Cosmological model-independent test of Λ CDM with two-point diagnostic by the observational Hubble parameter data. Eur. Phys. J. C **78**, 1 (2018). https://doi.org/10.1140/epjc/s10052-018-5796-y
86. O. Farooq, B. Ratra, Hubble parameter measurement constraints on the cosmological deceleration–acceleration transition redshift. Astrophys. J. Lett. **766**, L7 (2013)
87. V.H. Cárdenas, D. Grandón, S. Lepe, Dark energy and dark matter interaction in light of the second law of thermodynamics. Eur. Phys. J. C **79**, 357 (2019). arXiv:1812.03540 [astro-ph.CO]
88. S. Lepe, G. Otalora, Gauss–Bonnet dark energy on Hořava–Lifshitz cosmology. Eur. Phys. J. C **78**, 331 (2018). arXiv:1801.04213 [gr-qc]
89. L. Amendola, M. Quartin, S. Tsujikawa, I. Waga, Challenges for scaling cosmologies. Phys. Rev. D **74**, 023525 (2006). arXiv:astro-ph/0605488
90. G. Otalora, Scaling attractors in interacting teleparallel dark energy. JCAP **1307**, 044 (2013). arXiv:1305.0474 [gr-qc]
91. L. Amendola, Coupled quintessence. Phys. Rev. D **62**, 043511 (2000). arXiv:astro-ph/9908023
92. N. Mirabolfathi, Dark matter direct detection with low temperature detectors, in *48th Rencontres de Moriond on Electroweak Interactions and Unified Theories* (2013), pp. 123–130. arXiv:1308.0044 [astro-ph.IM]
93. D. Obreschkow, C. Power, M. Bruderer, C. Bonvin, A robust measure of cosmic structure beyond the power-spectrum: cosmic filaments and the temperature of dark matter. Astrophys. J. **762**, 115 (2013). arXiv:1211.5213 [astro-ph.CO]
94. P.-J. Wu, Y. Shao, S.-J. Jin, X. Zhang, A path to precision cosmology: synergy between four promising late-universe cosmological probes. JCAP **06**, 052 (2023). arXiv:2202.09726 [astro-ph.CO]
95. Z.-W. Zhao, L.-F. Wang, J.-G. Zhang, J.-F. Zhang, X. Zhang, Probing the interaction between dark energy and dark matter with future fast radio burst observations. JCAP **04**, 022 (2023). arXiv:2210.07162 [astro-ph.CO]
96. A. Cid, C. Rodriguez-Benites, M. Cataldo, G. Casanova, Bayesian comparison of interacting modified holographic Ricci dark energy scenarios. Eur. Phys. J. C **81**, 31 (2021)
97. C. Rodriguez-Benites, M. Cataldo, M. Vásquez-Arteaga, Universe with holographic dark energy. Momento 1 (2020)
98. C. Zhang, H. Zhang, S. Yuan, S. Liu, T.-J. Zhang, Y.-C. Sun, Four new observational h (z) data from luminous red galaxies in the Sloan Digital Sky Survey data release seven. Res. Astron. Astrophys. **14**, 1221 (2014)
99. J. Simon, L. Verde, R. Jimenez, Constraints on the redshift dependence of the dark energy potential. Phys. Rev. D **71**, 123001 (2005)
100. M. Moresco, A. Cimatti, R. Jimenez, L. Pozzetti, G. Zamorani, M. Bolzonella, J. Dunlop, F. Lamareille, M. Mignoli, H. Pearce et al., Improved constraints on the expansion rate of the universe up to z 1.1 from the spectroscopic evolution of cosmic chronometers. J. Cosmol. Astropart. Phys. **2012**(08), 006 (2012)
101. A.J. Cuesta, M. Vargas-Magaña, F. Beutler, A.S. Bolton, J.R. Brownstein, D.J. Eisenstein, H. Gil-Marín, S. Ho, C.K. McBride, C. Maraston et al., The clustering of galaxies in the SDSS-III baryon oscillation spectroscopic survey: baryon acoustic oscillations in the correlation function of LOWZ and CMASS galaxies in data release 12. Mon. Not. R. Astron. Soc. **457**, 1770 (2016)
102. C. Blake, S. Brough, M. Colless, C. Contreras, W. Couch, S. Croom, D. Croton, T.M. Davis, M.J. Drinkwater, K. Forster et al., The WiggleZ Dark Energy Survey: joint measurements of the expansion and growth history at $z < 1$. Mon. Not. R. Astron. Soc. **425**, 405 (2012)
103. A. Ratsimbazafy, S. Loubser, S. Crawford, C. Cress, B. Bassett, R. Nichol, P. Väisänen, Age-dating luminous red galaxies observed with the Southern African Large Telescope. Mon. Not. R. Astron. Soc. **467**, 3239 (2017)
104. D. Stern, R. Jimenez, L. Verde, M. Kamionkowski, S.A. Stanford, Cosmic chronometers: constraining the equation of state of dark energy. I: H (z) measurements. J. Cosmol. Astropart. Phys. **2010**(02), 008 (2010)
105. M. Moresco, Raising the bar: new constraints on the Hubble parameter with cosmic chronometers at $z \sim 2$. Mon. Not. R. Astron. Soc. **450**, L16 (2015)
106. T. Delubac, J.E. Bautista, J. Rich, D. Kirkby, S. Bailey, A. Font-Ribera, A. Slosar, K.-G. Lee, M.M. Pieri, J.-C. Hamilton et al., Baryon acoustic oscillations in the Lyα forest of BOSS DR11 quasars. A&A **574**, 59 (2015)
107. A. Font-Ribera, D. Kirkby, J. Miralda-Escudé, N.P. Ross, A. Slosar, J. Rich, É. Aubourg, S. Bailey, V. Bhardwaj, J. Bautista et al., Quasar-Lyman α forest cross-correlation from BOSS DR11: baryon acoustic oscillations. J. Cosmol. Astropart. Phys. **05**, 027 (2014)